Full Papers
doi.org/10.1002/ejic.202000895

Versatile Coordination Behavior of the Asymmetric Bis(3-mesityl-pyrazol-1-yl)(5-mesitylpyrazol-1-yl) Hydroborate Ligand towards Late 3d M^{2+} Ions

Lars Müller,[a] Vincent L. Nadurata,[b] Beatrice Cula,[a] Santina Hoof,[a] Christian Herwig,[a] and Christian Limberg*[a]

Bearing in mind the potential which tris(pyrazolyl) hydroborate ligands have demonstrated in various different fields of coordination chemistry, the behavior of a more rarely employed representative, namely bis(3-mesitylpyrazol-1-yl)(5-mesitylpyrazol-1-yl) hydroborate ($Tp^{Mes,H*}$), towards a series of divalent metal ions has been investigated. Thus, the synthesis of two new heteroleptic metal chlorido [$Tp^{Mes,H*}MCl$] complexes, **2**, (Mn^{2+}, **2-a**, and Cu^{2+}, **2-e**) are described, which correspond to the typical precursor compounds that would be needed for subsequent research. Structural and spectroscopic properties of the two new and four published members of this series (M = Fe^{2+}, **2-b**, Co^{2+}, **2-c**, Ni^{2+}, **2-d**, Zn^{2+}, **2-f**) are discussed in detail for the solid and solution states. Furthermore, synthetic routes to five homoleptic [$(Tp^{Mes,H*})_2M$] complexes, **3**, bearing Mn^{2+}, **3-a**, Fe^{2+}, **3-b**, Co^{2+}, **3-c**, Ni^{2+}, **3-d**, and Cu^{2+}, **3-e**, ions as well as an alternative preparation method for [$(\kappa^2$-$Tp^{Mes,H*})_2Zn$], **3-f**, are described. Their structures and spectroscopic parameters are compared to those of their heteroleptic counterparts. Additionally, the complex [$(Tp^{H,Mes*})_2Cu$], **4**, is reported, representing the second example of a complex with the (3-mesitylpyrazol-1-yl) bis(5-mesitylpyrazol-1-yl) hydroborate ligand ($Tp^{H,Mes*}$).

Introduction and Review

Since their first description in 1966 by Trofimenko, numerous derivatives of poly(pyrazolyl) borates (bis(pyrazol-1-yl) dihydroborate (Bp), tris(pyrazol-1-yl) hydroborate (Tp) and tetra(pyrazol-1-yl) borate (Tkp)) with different substitution patterns were published and an even larger number of main group and transition metal complexes was prepared.[1] Depending on the substitution pattern in the 3-, 4- and 5-position of the pyrazolyl groups, the steric and electronic properties can be tuned over a wide range, which has rendered them rather popular ligand systems in various different areas. For instance, Tp complexes have been serving as excellent spectroscopic, structural and functional model compounds for non-heme metal enzymes with $(His)_3$ or $(His)_2$(Carboxylate) binding sites.[2–5] In recent years, isomorphous substitution of native metal ions in such enzymes by ions of similar size and charge has become an often applied strategy in bioinorganic chemistry for further characterization and/or modification of the reactivity.[6] Hence, a profound knowledge on the preferred coordination environment of each applied metal ion is rather desirable to facilitate structural and spectroscopic characterization of metalloenzymes,[7–9] and the investigation of models can provide valuable information in this context. Given that Tp ligands have proved useful mimics of the abovementioned binding pockets, there is thus general interest in the complexation behavior in dependence on the central metal ion, and we decided to perform a systematic investigation on a representative that so far has been employed only rarely but bears a lot of potential. Before describing this choice, the state-of-the-art concerning homoleptic Tp complexes is outlined below.

$Tp^{R,R'}$ ligands (tris(3-R-5-R'-pyrazol-1-yl) hydroborate) offer three potential nitrogen donor atoms in a facial orientation and with an overall negative charge. With divalent first row transition metal ions, the formation of homoleptic complexes [$(Tp^{R,R'})_2M$] with C_{3v} symmetry and octahedral coordination geometry is highly preferred (**A**), although other coordination modes such as fivefold (**B**) or fourfold coordination (**C**) are feasible, too (Figure 1).[10,11] A selection of homoleptic Tp complexes published so far is depicted in Table 1. Several trends can be identified by examining the metal-nitrogen bond distances. They decrease with higher atomic number of the central metal atom, following the trend of transition metal ion size. By introduction of methyl groups in the 3-position of the pyrazolyl donors, the metal-nitrogen bonds are elongated due to the higher steric demand of these residues. In general, the three metal-nitrogen distances are almost equal except in

[a] L. Müller, Dr. B. Cula, Dr. S. Hoof, Dr. C. Herwig, Prof. Dr. C. Limberg
Institut für Chemie
Humboldt-Universität zu Berlin
Brook-Taylor-Straße 2, 12489 Berlin, Germany
E-mail: christian.limberg@chemie.hu-berlin.de
https://www.chemie.hu-berlin.de/aglimberg/
[b] V. L. Nadurata
School of Chemistry
University of Melbourne
Parkville, Victoria 3010, Australia

Supporting information for this article is available on the WWW under https://doi.org/10.1002/ejic.202000895

Part of the joint "German Chemical Society ADUC Prizewinner" Collection with EurJOC.

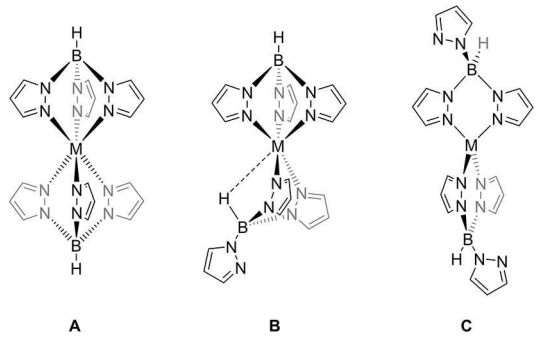

Figure 1. Different coordination modes of Tp ligands found in homoleptic transition metal complexes [Tp_2M]: **A**: κ^3,κ^3, **B**: κ^2,κ^3, **C**: κ^2,κ^2. Substituents at the pyrazolyl donors were omitted for clarity.

copper(II) complexes, where a *Jahn-Teller* distortion occurs. The *Jahn-Teller* distortion becomes less evident with increasing steric demand of the substituents in the 3-position.

With phenyl residues in the 3-position of the pyrazolyl donors, the metal-nitrogen bond distances increase further and the formation of homoleptic complexes becomes less favorable. In general, there are two ways, through which the systems can minimize the steric congestion imposed by the phenyl residues.

(i) The coordination number of the metal decreases to fivefold coordination, as is found for [$(Tp^{Ph,H})_2$Co], **IV-c**, and [$(Tp^{Ph,4CN})_2$Co], **VI-c**, ($Tp^{Ph,4CN}$ = tris(4-cyano-3-phenylpyrazol-1-yl) hydroborate), where one Tp ligand coordinates in an κ^3- and the other in an κ^2-binding mode.[12,13] The sixth coordination site is then often occupied by the borohydride atom of the κ^2-bound Tp ligand resulting in a weak interaction between hydrogen atom and metal (see **B** in Figure 1). This kind of M···HB bond is known also from other polypyrazolyl borate ligand combinations, e.g. both from homoleptic [$(Bp^{R,R'})_2$M] complexes[14–19] and mixed ligand [$(Bp^{R,R'})(Tp^{R'',R'''})$M] systems[13,20–22] involving cobalt(II) and other late-transition metal ions. In some complexes, these distances are quite short and the coordination might as well be considered as octahedral. With the even smaller zinc(II) ion distorted tetrahedral complexes with κ^2-coordination of both Tp ligands are formed (see **C** in Figure 1), as observed for [$(Tp^{Ph,H})_2$Zn], **IV-f**,[23] and [$(Tp^{Mes,H*})_2$Zn], **3-f.**[24] **3-f** was reported to form in very low yield as an adventitious product from [$Tp^{Mes,H*}$ZnEt] in benzene over one-week.[24] Besides the results of an X-ray structure analysis no other spectroscopic data were provided.

(ii) The second way for the system to circumvent steric constraints is ligand isomerization. This has been observed for [$(Tp^{Ph,Me})_2$M] (M = Co^{II}, Cu^{II}) complexes, **V**, which isomerize to the respective asymmetric [$(Tp^{Ph,Me*})_2$M] compounds **V′-c** (M = Co), **V′-e** (M = Cu) (Scheme 1). As a result of this rearrangement, the average metal nitrogen bond distance slightly shortens and the symmetry decreases from C_{3v} to C_s. In case of copper(II), the lower symmetry structure appears to be strongly favored considering that exclusively **V′-e** and not **V-e** has been described in literature. The respective iron(II) and nickel(II) complexes **V-b** and **V-d** retain their constitution, while in the case of cobalt(II), both isomers **V-c** and **V′-c** could be structurally characterized.

Similar spontaneous rearrangements were observed in attempts to prepare complexes with the $Tp^{Ph,4CN}$ ligand. Only in

Table 1. Selected homoleptic Tp complexes with M–N and M···HB distances (in Å) and coordination modes of the ligands.

	Mn	Fe	Co	Ni	Cu	Zn
I: [Tp_2M]	**I-a**,[29] κ^3,κ^3 2.263, 2.197, 2.265; 2.223, 2.285, 2.272	**I-b**,[30][a] κ^3,κ^3 1.973, 1.980, 1.972; 1.979, 1.960, 1.971	**I-c**,[31] κ^3,κ^3 2.123, 2.120, 2.130; 2.133, 2.128, 2.140	**I-d**,[32] κ^3,κ^3 2.11 (average)	**I-e**,[33] κ^3,κ^3 2.018, 2.528, 1.991	**I-f**,[34] κ^3,κ^3 2.148, 2.150, 2.162; 2.152, 2.175, 2.143
II: [$(Tp^{Me,H})_2$M]	**II-a**	**II-b**,[35] κ^3,κ^3 2.197, 2.200, 2.201	**II-c**,[36] κ^3,κ^3	**II-d**,[37] κ^3,κ^3 2.101, 2.134, 2.106	**II-e**,[33] κ^3,κ^3 2.112, 2.342, 2.024	**II-f**[37] [b]
III: [$(Tp^{Me2})_2$M]	**III-a**[38], κ^3,κ^3 2.270	**III-b**[30], κ^3,κ^3 2.190, 2.179, 2.147	**III-c**[36], κ^3,κ^3	**III-d**[39], κ^3,κ^3 2.142, 2.106, 2.137	**III-e**[40], κ^3,κ^3 2.140, 2.013, 2.252; 2.113. 2.042, 2.324	**III-f**[41], κ^3,κ^3 2.160, 2.175, 2.197
IV: [$(Tp^{Ph,H})_2$M	**IV-a**[42], κ^3,κ^3 2.310, 2.329, 2.310	**IV-b**[42], κ^3,κ^3 2.265, 2.237, 2.242; 2.240, 2.244, 2.248	**IV-c**[12], κ^2,κ^3 2.103, 2.138, 2.199, 2.124[c], 2.201[c], 2.17[e]		**IV-e**[43], [b]	**IV-f**[23], κ^2,κ^2 2.007, 2.018
V: [$(Tp^{Ph,Me})_2$M]		**V-b**[44], κ^3,κ^3 2.218, 2.270, 2.233	**V-c**[45], κ^3,κ^3 2.169, 2.200, 2.271	**V-d**[46], κ^3,κ^3 2.149, 2.157, 2.226		
V′: [$(Tp^{Ph,Me*})_2$M]			**V′-c**[45], κ^3,κ^3 2.260, 2.206, 2.113[d]; 2.148[d], 2.239, 2.172		**V′-e**[45], κ^3,κ^3 2.158, 2.180, 2.240[d]; 2.118, 2.216, 2.255[d]	
VI: [$(Tp^{Ph,4CN})_2$M]			**VI-c**[13], κ^2,κ^3 2.099, 2.131, 2.229, 2.107[c], 2.097[c], 2.507[e]			
VI′: [$(Tp^{Ph,4CN*})_2$M]	**VI′-a**[25], κ^3,κ^3 2.160, 2.160, 2.309[d]	**VI′-b**[25], κ^3,κ^3 2.043, 2.043, 2.256[d]	**VI′-c**[25], κ^3,κ^3 2.042, 2.042, 2.226[d]			
3: [$(Tp^{Mes,H*})_2$M]	**3-a**, κ^2,κ^3 2.230, 2.300, 2.164[d], 2.240, 2.160[d], 2.550[e]	**3-b**, κ^2,κ^3 2.132, 2.248, 2.084[d], 2.179, 2.084[d], 2.310[e]	**3-c**, κ^2,κ^3 2.086, 2.256, 2.054[d], 2.125, 2.039[d], 2.334[e]	**3-d**, κ^2,κ^3 2.075, 2.148, 2.012[d], 2.110, 2.032[d], 2.195[e]	**3-e**, κ^2,κ^2 1.994, 1.930[d], 1.986, 1.926[d]	**3-f**[24], κ^2,κ^2 2.003, 1.958[d]

[a] Low-spin complex. [b] Only spectroscopic characterization. [c] κ^2-coordinating nitrogen donors. [d] By 1,2-borotropic rearrangement deviating pyrazolyl donor. [e] M···HB distances.

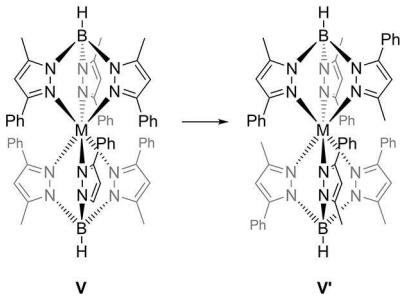

Scheme 1. Spontaneous ligand rearrangement of $Tp^{Ph,Me}$ by 1,2-borotropic shift in transition metal complexes $[(Tp^{Ph,Me})_2M]$, **V**, (C_{3v} symmetry) to form the respective complexes with reduced symmetry (C_s) $[(Tp^{Ph,Me*})_2M]$, **V'**.

case of cobalt(II) a complex could be isolated that contained Tp ligands with the initial connectivity, bound in a κ^2,κ^3-coordination, namely $[(Tp^{Ph,4CN})_2Co]$, **VI-c**, as described above. For the other metal ions, rearrangements occurred resulting in the products $[(Tp^{Ph,4CN*})_2M]$, **VI'-a** (M = Mn), **VI'-b** (M = Fe), **VI'-c** (M = Co).[25] A mechanism for the 1,2-borotropic rearrangement was proposed.[13]

Coming now back to our choice of a Tp ligand for a comprehensive study, the following thoughts were considered. For biomimetic model studies with Tp complexes especially ligands with sterically demanding substituents in the 3-position of the pyrazolyl donors were applied to simulate hydrophobic binding pockets. In this context, mesityl residues have been shown to establish an interesting balance between protection and space for reactivity at the metal center in $Tp^{Mes,H}$ complexes, and recent work has demonstrated that using the variant with one 1,2-rearranged pyrazolyl unit ($Tp^{Mes,H*}$) leads to an increased reactivity due to a more open metal site (Figure 2).[26] Consequently, we have selected this more rarely used (and likely undervalued) ligand to study its coordination chemistry with various metals, the resulting structures and the spectroscopic properties.

More concretely, we describe the synthesis of two new heteroleptic metal chlorido $[Tp^{Mes,H*}MCl]$ complexes, **2**, which correspond to the typical precursor compounds that would be needed for subsequent research; this may of course include biomimetic studies[26] but it is also worth mentioning that comparable compounds proved active catalysts in olefin oligo- and polymerizations.[27,28] While we and others have already reported representatives with M = Fe^{2+}, Co^{2+}, Ni^{2+} and Zn^{2+}, we here extend the series with Mn^{2+}, **2-a**, and Cu^{2+}, **2-e** as central metal ions.

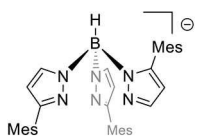

Figure 2. Bis(3-mesitylpyrazol-1-yl)(5-mesitylpyrazol-1-yl) hydroborate ($Tp^{Mes,H*}$) with one 1,2-rearranged pyrazolyl unit.

Structural and spectroscopic properties of the two new and four known members of this series (M = Fe^{2+}, **2-b**, Co^{2+}, **2-c**, Ni^{2+}, **2-d**, Zn^{2+}, **2-f**) will be discussed in detail for the solid and solution states. Furthermore, synthetic routes to five homoleptic $[(Tp^{Mes,H*})_2M]$ complexes, **3**, bearing Mn^{2+}, **3-a**, Fe^{2+}, **3-b**, Co^{2+}, **3-c**, Ni^{2+}, **3-d**, and Cu^{2+}, **3-e**, ions as well as an alternative preparation method for $[(\kappa^2\text{-}Tp^{Mes,H*})_2Zn]$, **3-f**, are described. Their structures and spectroscopic parameters are compared to those of their heteroleptic counterparts. Additionally, the complex $[(Tp^{H,Mes*})_2Cu]$, **4**, is reported, representing the second example of a complex with the (3-mesitylpyrazol-1-yl)bis(5-mesitylpyrazol-1-yl) hydroborate ligand.[27] The latter is derived from $Tp^{Mes,H*}$ by the switching of a further pyrazolyl group such that the mesityl group shifts from the 3-position to the 5-position.

Results and Discussion

Synthesis

Bis(3-mesitylpyrazol-1-yl)(5-mesitylpyrazol-1-yl) hydroborate ($Tp^{Mes,H*}$) was initially described by Rheingold *et al.* in 1993 and represents the first example of an asymmetric Tp ligand.[47] It is formed as the main product along the synthesis of the symmetric ligand $Tp^{Mes,H}$ in a high temperature reaction between potassium borohydride and 3-mesityl pyrazole. Instead of synthesizing the respective thallium salts from the crude product and subsequently separating $TlTp^{Mes,H}$ and $TlTp^{Mes,H*}$, as described by Rheingold *et al*, we directly separated the initially formed potassium salts by fractionalized crystallization and used those in salt metathesis reactions to avoid the toxic thallium salts.

Starting from $KTp^{Mes,H*}$, **1**, six heteroleptic and six homoleptic complexes were prepared in metathesis reactions starting from metal dihalides. The resulting complexes, bearing the respective metal ions in oxidation state +II, (**2-a**, **3-a**: Mn^{2+}, **2-b**, **3-b**: Fe^{2+}, **2-c**, **3-c**: Co^{2+}, **2-d**, **3-d**: Ni^{2+}, **2-e**, **3-e**: Cu^{2+} and **2-f**, **3-f**: Zn^{2+}), were obtained selectively depending on reaction conditions and the stoichiometry of the reactants (Scheme 2). The synthesis of $[Tp^{Mes,H*}CuCl]$, **2-e**, followed the procedure we had already described for $[Tp^{Mes,H*}FeCl]$, **2-b**, and complex $[Tp^{Mes,H*}MnCl]$, **2-a**, was prepared analogously to $[Tp^{Mes,H*}CoCl]$, **2-c**.[26] The nickel and the zinc complex, $[Tp^{Mes,H*}NiCl]$, **2-d**, and $[Tp^{Mes,H*}ZnCl]$, **2-f**, had been reported previously[27,47] to form *via* a route involving the abovementioned toxic thallium precursors, but we were able to show that they can be accessed alternatively starting from nickel chloride hexahydrate or zinc chloride and $KTp^{Mes,H*}$. The homoleptic complexes $[(Tp^{Mes,H*})_2M]$, **3-a** (M = Mn), **3-b** (M = Fe), **3-c** (M = Co), **3-d** (M = Ni), and **3-f** (M = Zn) were formed when the stoichiometry was adjusted and the reaction mixtures were treated in an ultrasonic bath.

For the synthesis of $[(Tp^{Mes,H*})_2Cu]$, **3-e**, the potassium salt **1** was stirred with dispersed $CuCl_2$ in THF without ultrasound treatment. Under reaction conditions as applied for the other homoleptic complexes, partial isomerization of the ligand was

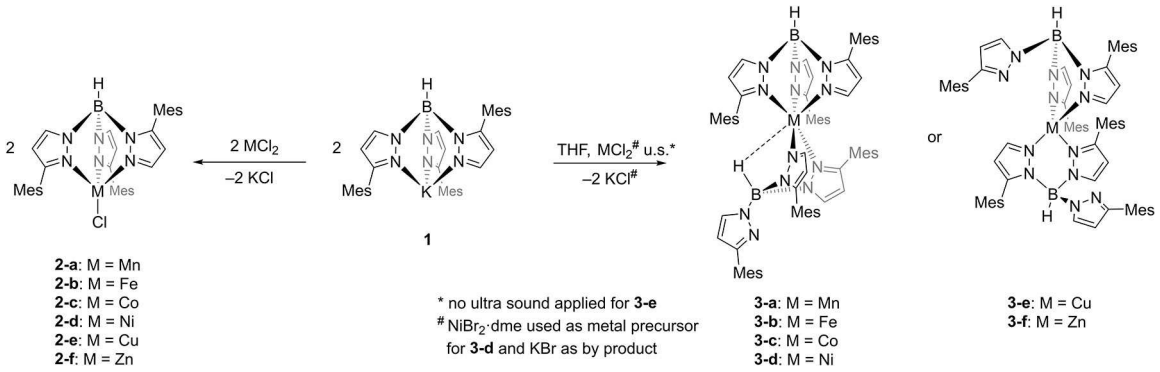

Scheme 2. Synthesis of the heteroleptic complexes [$Tp^{Mes,H*}$MCl] **2-a** to **2-f** and the homoleptic complexes [$(Tp^{Mes,H*})_2$M] **3-a** to **3-f** starting from potassium bis(3-mesitylpyrazol-1-yl)(5-mesitylpyrazol-1-yl) hydroborate, **1**.

observed and a mixture of the complexes **3-e** and [$(Tp^{H,Mes*})_2$Cu], **4**, was obtained (Scheme 2, Figure 3).

The yield of **3-e** in the reaction without ultrasound treatment is higher than the combined yields of **3-e** and **4** in the reaction with ultrasound treatment. This indicates that **4** is not formed from **3-e** in a straightforward fashion through the ultrasound and indeed there were indications for the formation of various by-products under these conditions, which, however, could be readily removed during work-up. Complexes **3-e** and **4** were very difficult to separate, though, as solubilities and spectroscopic properties did not differ significantly. However, single crystals of the two compounds could be distinguished by a slight color difference and thus separated manually.

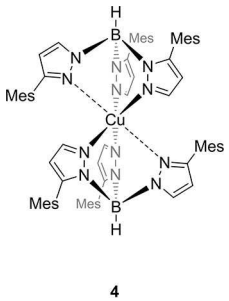

Figure 3. Copper complex [$(Tp^{H,Mes*})_2$Cu], **4**, obtained after ultrasonic treatment of $CuCl_2$ dispersed in THF with two equivalents potassium bis(3-mesitylpyrazol-1-yl)(5-mesitylpyrazol-1-yl) hydroborate, **1**.

Solid State Properties

Heteroleptic Complexes

The complexes **2-a**, **2-b** and **2-f** are colorless, while **2-c**, **2-d** and **2-e** are blue, salmon pink and ochre, respectively. Attenuated total reflection infrared spectroscopy (ATR-IR) of the heteroleptic complexes in the solid state show almost identical IR spectra with hardly any dependency of the B–H stretching vibration on the respective M^{2+} ion (2517 or 2518 cm^{-1}, only complex **2-a** deviates somewhat with 2489 cm^{-1}, Table 2).

The colored complexes undergo an immediate color change, even in the solid state, when a coordinating solvent like acetonitrile (MeCN) is present (Table 2). To gather information on the resulting complexes, single crystals of all representatives were grown to determine their structures by X-ray diffraction analysis. Cooling a hot MeCN solution of **2-a** afforded good quality crystals of the respective solvent adduct **2-a(MeCN)** (Figure S1). Single crystals of **2-d(MeCN)**·MeCN and **2-e(MeCN)**·MeCN, which additionally contained a co-crystallized MeCN molecule per complex molecule, were obtained by layering a concentrated solution of **2-d** and **2-e** in dichloro-

Table 2. Selected spectroscopic and structural properties of the heteroleptic complexes **2-a**, **2-b**, **2-c**, **2-d**, **2-e** and **2-f** and those of their corresponding acetonitrile adducts **2-a(MeCN)**, **2-b(MeCN)**, **2-c(MeCN)**, **2-d(MeCN)** and **2-e(MeCN).**

M^{2+}		color	ν(B–H) [cm^{-1}]		color	τ_4[a][48], τ_5[b][49]
Mn^{2+}	**2-a**	colorless	2489	**2-a(MeCN)**	colorless	0.63[b]
Fe^{2+}	**2-b**	colorless	2517[26]	**2-b(MeCN)**[c]	colorless	0.66[b][26]
Co^{2+}	**2-c**	blue	2517[26]	**2-c(MeCN)**[c]	purple	0.66[b][26]
Ni^{2+}	**2-d**	pink	2518 (2517[27])	**2-d(MeCN)**[c]	green	0.64[b]
Cu^{2+}	**2-e**	ochre	2517	**2-e(MeCN)**[c]	blue	0.53[b]
Zn^{2+}	**2-f**	colorless	2518 (2515[47])	**2-f**[c]	colorless	0.73[a]

[a] τ_4. [b] τ_5. [c] Crystallized together with an additional non-coordinating molecule of MeCN: **2-b(MeCN)**·MeCN, **2-c(MeCN)**·MeCN, **2-d(MeCN)**·MeCN, **2-e(MeCN)**·MeCN, **2-f**·2MeCN.

methane (DCM) with MeCN (Figure S2, Figure S3); they are isostructural to the published complexes **2-b(MeCN)**·MeCN and **2-c(MeCN)**·MeCN.[26] In all structures the metal center features a coordination sphere composed of three pyrazolyl nitrogen donors belonging to the Tp ligand, one acetonitrile ligand and one chlorido ligand. The coordinated MeCN can be easily removed by applying extended *vacuo* conditions except for **2-a (MeCN)** where the MeCN molecule remains bound even under high vacuum conditions (10^{-7} mbar) (Scheme 3).

Only **2-f** has no tendency to form an acetonitrile adduct; under conditions that lead to the acetonitrile adducts in case of the other complexes the Zn atom retains the tetrahedral coordination sphere already observed by Rheingold *et al.* and crystallizes without bound solvent but with two equivalents of non-coordinating MeCN molecules in the unit cell (**2-f**·2MeCN) (Figure S4).[47]

The M–N bond lengths of complexes **2-a(MeCN)** to **2-d (MeCN)**·MeCN do not differ significantly and correspond well to the calculated sums of ionic radii, which necessarily follow the size trend of the M^{2+} metal ions in fivefold coordination (Figure 4 a)).[50] The two nitrogen atoms N7 and N5 span the largest N–M–N angle, and consequently the M–N5 distance is slightly larger than the other two metal-pyrazolyl distances, as the acetonitrile ligand exerts a trans influence on the pyrazole unit in trans position. The M–Cl bond is in all cases somewhat shorter than the sum of the ionic radii indicating a strong covalent contribution. The structural parameter τ_5[49] varies in a small range between 0.63 (**2-a(MeCN)**) and 0.66 (**2-b(MeCN)**·MeCN, **2-c(MeCN)**·MeCN), indicating that the coordination sphere should be described rather as trigonal bipyramidal than as square pyramidal (Table 2). The d^5 system **2-a(MeCN)** represents the structure with lowest steric strain due to lacking effects of ligand field stabilization energy (LFSE). Still, the geometric index is not as high as for an ideal trigonal bipyramid due to the facial orientation of the pyrazolyl donors, which does not allow for N1–M–N3 angles larger than 90°. A perfect trigonal bipyramidal coordination can therefore never be reached with the Tp ligand. The structures and geometric indices of **2-b(MeCN)**·MeCN, **2-c(MeCN)**·MeCN and **2-d(MeCN)**·MeCN are almost identical to those of **2-a(MeCN)**, which indicates that the structures are mainly governed by steric and electrostatic aspects rather than electronic effects.[51] The geometry parameter of the copper complex **2-e(MeCN)**·MeCN is with 0.53 somewhat lower, indicating a distinct square pyramidal coordination (Table 2). The Cu–N1 bond is significantly elongated (Figure 4a, Figure 4b). The clearly differing bond lengths and angles found in **2-e(MeCN)**·MeCN can only be explained when electronic effects are additionally taken into account. A *Pseudo Jahn-Teller* distortion[52,53] is a reasonable explanation as it is similarly observed in the solid state structure of CuX_5^{2-} anions (X = Cl^-, Br^-, NCS^-) extensively discussed by Reinen *et al.*[51,54,55] The fact that complex **2-f** avoids coordination of MeCN and adopts a tetrahedral coordination of the Zn^{2+} ion can also be explained by means of *Pseudo Jahn-Teller* distortion as outlined for the example of the $ZnCl_4^{2-}$ anion in $[Co(NH_3)_6][ZnCl_4]Cl$.[51,56]

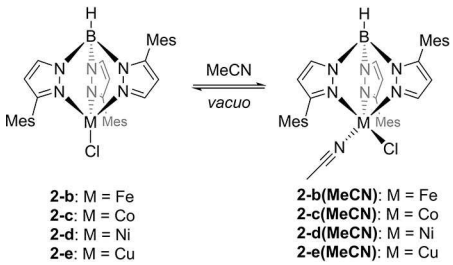

Scheme 3. Reversible coordination of MeCN to the heteroleptic complexes **2-b**, **2-c**, **2-d** and **2-e**.

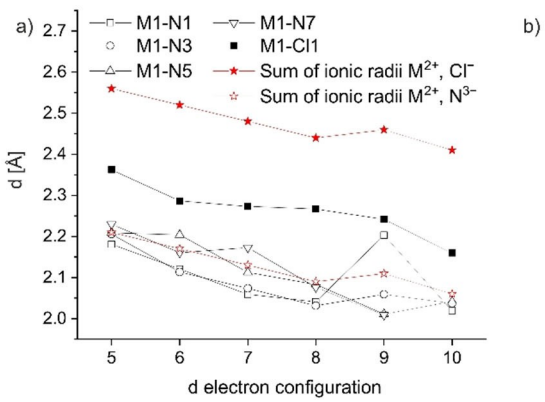

Figure 4. a) Selected bond lengths found in the solid state structures in dependency on the d electron configuration compared with theoretical values calculated on basis of ionic radii; ionic radii CN = 4 (Zn^{2+}, N^{3-}), CN = 5 (Mn^{2+}, Fe^{2+} intrapolated, Co^{2+}, Ni^{2+}, Cu^{2+}), CN = 6 (Cl^-);[50] b) molecular structure of [$Tp^{Mes,H*}$Cu(NCMe)Cl], **2-e(MeCN)**·MeCN, as determined by single crystal X-ray diffraction, non-coordinating solvent molecules and hydrogen atoms except the one bound to boron were omitted for clarity, selected bond length (in Å) and angles (in °): Cu1-N1 = 2.2031(19), Cu1-N3 = 2.0589(18), Cu1-N5 = 2.0112(18), Cu1-N7 = 2.0088(19), Cu1-Cl1 = 2.2416(9), N1-Cu1-N7 = 91.97(7), N3-Cu1-N7 = 91.67(7), N5-Cu1-N7 = 179.33(7), N1-Cu1-Cl1 = 125.37(5) N3-Cu1-Cl1 = 147.69(5).

Homoleptic Complexes

The homoleptic complexes **3-a**, **3-b** and **3-f** are colorless powders, while **3-c**, **3-d** and **3-e** are lilac, blue and green, respectively (Table 3). The effective magnetic moments of **3-a**, **3-b**, **3-c**, **3-d** and **3-e** correspond well to the spin-only values of d^5, d^6, d^7, d^8 and d^9 configurations in high-spin states (Table S3). Small deviations can be explained by a limited contribution of spin-orbit coupling to the magnetic moment. Complex **3-f** proved to be diamagnetic as expected for a d^{10} complex (see Figure S19, Table S3). The Mößbauer spectrum of complex **3-b** measured for a powder sample at 14 K is also in line with a high-spin configuration ($\delta = 1.07$ mm/s, $\Delta E_q = 3.78$ mm/s, Figure S37).

For all six homoleptic complexes **3-a** to **3-f**, single crystals suitable for X-ray diffraction could be grown by layering either a concentrated THF solution with diethyl ether or a concentrated DCM solution with acetonitrile. Complexes **3-b** and **3-e** crystallize with 0.5 and 2 equivalents of non-coordinating DCM in the unit cell, respectively (**3-b**·0.5CH_2Cl_2, **3-e**·2CH_2Cl_2). In complexes **3-a**, **3-b**, **3-c** and **3-d** the metal centers are coordinated by one $Tp^{Mes,H*}$ ligand in a κ^3-mode and the second one in a κ^2-mode, so that five coordination sites are occupied (Figure 5 a, Figure S5 to Figure S7). The sixth coordination site is occupied by a B–H hydride atom (belonging to the latter $Tp^{Mes,H*}$ ligand), which is oriented towards the metal center, resulting in a pseudo-octahedral coordination sphere. Examples where two equal Tp ligands are bound to one metal center in differing ways are rare in the literature and no precedent cases for manganese, iron and nickel complexes have been reported so far (Table 1).

The M–N distances for complexes **3-a** to **3-d** generally correspond to the sum of ionic radii of the respective pentacoordinated M^{2+} ions and nitrogen with coordination number 4 (Figure 6). As observed for the heteroleptic complexes, the M–N distances involving the two donors spanning the largest N–M–N angle are slightly larger than the others. The M···HB distance is largest for the manganese complex **3-a** with 2.550 Å and shortest for the nickel complex **3-d** with 2.195 Å (Table 3). Of course, no conclusion about the nature of the corresponding interactions can be drawn solely based on metal hydrogen distances and structural parameters. M···HB distances observed in the past for homoleptic Bp or mixed ligand Tp complexes are in a similar range between 1.86 and 2.36 Å.[12–14,58] For comparison, hydrogen metal distances in agostic M···HC interactions (3C2E) range between 1.8 and 2.3 Å, whereas anagostic interactions (3C4E) are characterized by larger distances, ranging between 2.3 and 2.9 Å.[59,60] However, a 3C2E bond can be excluded as this would require an empty *d*-orbital that is not available in case of high-spin complexes with the metal ions considered here, and in fact, on the contrary, a strengthening of the M···HB interaction becomes evident from manganese(II) over iron(II) and cobalt(II) to nickel (II). The interactions will thus be electrostatic in nature, involving filled or half-filled orbitals. Nevertheless, the short metal borohydride distance indicates an attractive rather than a repulsive interaction, which might promote the observed pentagonal coordination.

The geometry index τ_5 shows the highest value for **3-a** (0.494), indicating a more trigonal bipyramidal coordination, which is in line with the longest M···HB distance.[49] The τ_5 values for complexes **3-b**·0.5CH_2Cl_2 and **3-c** are almost identical (0.340, 0.337), and smallest for complex **3-d** (0.276), which again fits to the observation made for the M···HB distances (Table 3).

In contrast to the complexes with d^5 to d^8 electron configuration, in the complexes **3-e**·2CH_2Cl_2 and **3-f** a fourfold coordination of the metal ions by the pyrazolyl donors of two $Tp^{Mes,H*}$ ligands bound in a κ^2-coordination mode is found (Figure 5b, Figure 5c). While the ligand arrangement can be described as tetrahedral in the case of the zinc complex ($\tau_4 = 0.859$), the coordination sphere of the copper complex is more distorted with a τ_4 value of 0.610 (Table 3).[48] In both cases the M–N bonds are slightly shorter, compared to the sum of ionic radii of M^{2+} and N^{3-} (both with coordination number four). The d^9 and d^{10} configuration seems to disfavor an attractive metal borohydride interaction, resulting in distorted tetrahedral coordinations. The tetragonal distortion found in **3-e**·2CH_2Cl_2 can be explained by a *Jahn-Teller* distortion frequently found in fourfold coordinated Cu^{2+} complexes.[53]

To estimate to what extend steric congestion – rather than electronic effects – is responsible for the structure of the homoleptic complexes, the software Solid-G[57] was used. The volume of unfavorable close contact of the ligands, the percentage of the metal's surface shielded by the ligated

Table 3. Selected solid state properties of the homoleptic $[(Tp^{Mes,H*})_2M]$ complexes **3-a**, **3-b**, **3-c**, **3-d**, **3-e** and **3-f** and of $[(Tp^{H,Mes*})_2Cu]$, **4**, including color, M···HB distance, percentage of the metal's surface shielded by the ligated atoms only (G(M)) and percentage of the sphere shielded by both ligands (G(comp.)) determined with the software Solid-G[57] and τ_4[48] and τ_5[49] values.

M		color	ν(B–H) [cm^{-1}]	M···HB [Å]	G(M) [%]	G(comp.) [%]	τ_4[a][48], τ_5[b][49]
Mn	**3-a**	colorless	2489	2.550	67.69	90.16	0.49[b]
Fe	**3-b**[c]	colorless	2480	2.310	73.11	94.89	0.34[b]
Co	**3-c**	lilac	2481	2.334	75.69	95.81	0.34[b]
Ni	**3-d**	blue	2485	2.195	78.29	96.79	0.28[b]
Cu	**3-e**[c]	green	2451	-	73.10	96.62	0.61[a]
Zn	**3-f**	colorless	2482	-	71.99	97.12	0.86[a]
Cu	**4**[c]	light green	-	-	78.09	97.12	[d]

[a] τ_4. [b] τ_5. [c] Crystallized with non-coordinating solvent molecules in the unit cell **3-b**·0.5CH_2Cl_2, **3-e**·2CH_2Cl_2, **4**·2MeCN. [d] *Jahn-Teller* distorted O_h coordination.

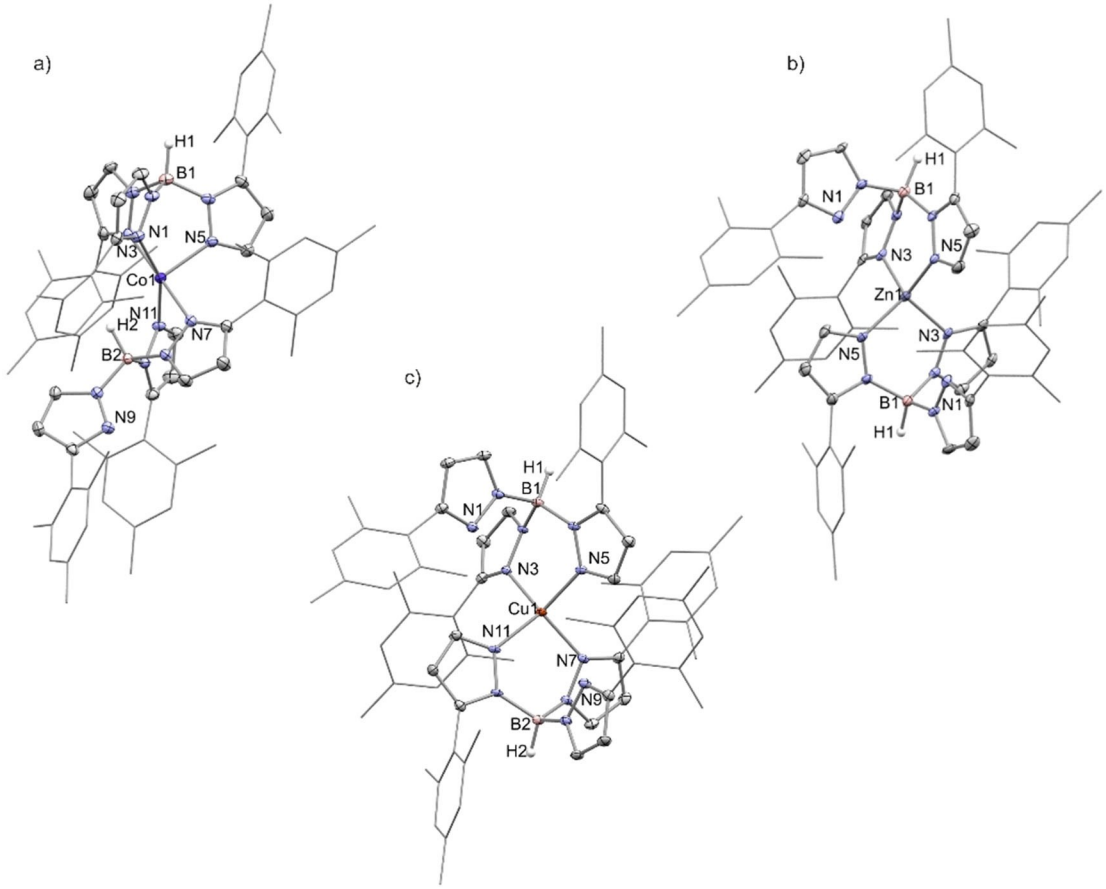

Figure 5. Molecular structures as determined by single crystal X-ray diffraction of a) [$(Tp^{Mes,H*})_2Co$], **3**-**c**, selected bond length (in Å) and angles (in °): Co1-N1 = 2.0863(16), Co1-N3 = 2.2557(16), Co1-N5 = 2.0539(17), Co1-N7 = 2.1252(16), Co1-N11 = 2.0386(16), Co1-H2 = 2.334, N1-Co1-N11 = 157.43(7), N3-Co1-N7 = 177.67(6); b) [$(Tp^{Mes,H*})_2Zn$], **3**-**f**, selected bond length (in Å) and angles (in °): Zn1-N3 = 2.003(4), Zn1-N5 = 1.958(4), N3-Zn1-N3 = 111.9(2), N5-Zn1-Zn5 = 127.0(3); c) [$(Tp^{Mes,H*})_2Cu$], **3**-**e**·$2CH_2Cl_2$, selected bond length (in Å) and angles (in °): Cu1-N3 = 1.994(2), Cu1-N5 = 1.930(2), Cu1-N7 = 1.986(2), Cu1-N11 = 1.926(2), N5-Cu1-N11 = 141.13(9), N3-Cu1-N7 = 132.79(9), non-coordinating solvent molecules and hydrogen atoms except for the ones bound to boron atoms were omitted for clarity.

atoms only (G(M)) and percentage of the sphere shielded by both ligands (G(comp.)) was determined (Table 3). The visualization of these results was performed with SolidAngleGL8 and can be found in the Supporting Information (Figure S8). None of the calculations revealed unfavorable close contacts between the two ligands. G(M) values range between 67.69% for **3**-**a** and 78.29% for **3**-**d**. Surprisingly, the shieldings of the tetrahedrally coordinated metal centers is with 73.10% and 71.99% for **3**-**e**·$2CH_2Cl_2$ and **3**-**f**, respectively, not much smaller than those of the fivefold coordinated metal centers (Table 3). G(comp.) differs even less: all values lie within a range between 90.16% (**3**-**a**) and 97.12% (**3**-**f**), which means that all metal centers are almost entirely shielded by the $Tp^{Mes,H*}$ ligands. The benefits in terms of steric congestion of tetrahedral *vs.* pentagonal coordination are rather small, emphasizing the importance of other factors such as stabilizing metal borohydride interactions and the *(Pseudo) Jahn-Teller* effect. Notably, the herein reported copper(II) complex **3**-**e** is the first example of a homoleptic Tp complex with a coordination environment differing from the one of a *Jahn-Teller* distorted octahedron.

Such a *Jahn-Teller* distorted octahedral coordination is found for the copper ion in complex [$(Tp^{H,Mes*})_2Cu$], **4**, which crystallizes as a solvate with two non-coordinating MeCN molecules in the unit cell (**4**·2MeCN). The axial M–N bonds are remarkably elongated and at 2.57 Å are the longest ones observed so far for homoleptic Tp copper complexes. They involve the two pyrazolyl donors with the bulky mesityl residues in the 3-position, which through binding at long distance reduce steric congestion, whereas the other four pyrazolyl donors – containing the mesityl residues in the 5-position and only protons in the 3-position – are arranged in the equatorial plane closer to the metal center. Only very few other Tp ligands are known where two bulky residues are found in the 5-position of the Tp ligand.[61] In fact, the herein presented complex **4** is only the second precedent case of a metal complex featuring the ligand $Tp^{H,Mes*}$ (Figure 7).[27] Complexes **3**-**e** and **4** can be considered as isomers, which are linked through a 1,2-borotropic ligand rearrangement. While comparable ligand rearrangements have been observed (vide supra), there is no other precedence, where, as

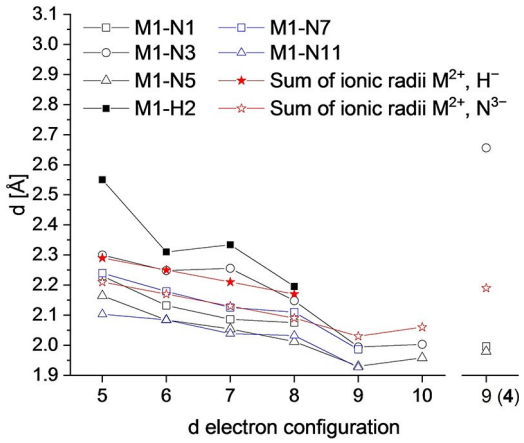

Figure 6. M···HB distances (in Å) found in the complexes $[(Tp^{Mes,H*})_2Mn]$, **3-a**, $[(Tp^{Mes,H*})_2Fe]$, **3-b**·0.5CH_2Cl_2, $[(Tp^{Mes,H*})_2Co]$, **3-c**, and $[(Tp^{Mes,H*})_2Ni]$, **3-d**, in dependency on the d electron configuration (filled black) compared with the sum of the ionic radii of the respective M^{2+}-ion in coordination number 5 and a hydride ion (filled red); M—N distances (in Å) found in the complexes $[(Tp^{Mes,H*})_2Mn]$, **3-a**, $[(Tp^{Mes,H*})_2Fe]$, **3-b**, $[(Tp^{Mes,H*})_2Co]$, **3-c**, $[(Tp^{Mes,H*})_2Ni]$, **3-d**, $[(Tp^{Mes,H*})_2Cu]$, **3-e**·2CH_2Cl_2, $[(Tp^{Mes,H*})_2Zn]$, **3-f**, and $[(Tp^{H,Mes*})_2Cu]$, **4**·2MeCN, (hollow black and hollow blue) compared with the sum of ionic radii of respective M^{2+} ion in coordination number 5 for **3-a** to **3-d** and in coordination number 4 for **3-e**, **3-f** and **4** and N^{3-} in coordination number 4 (hollow red).

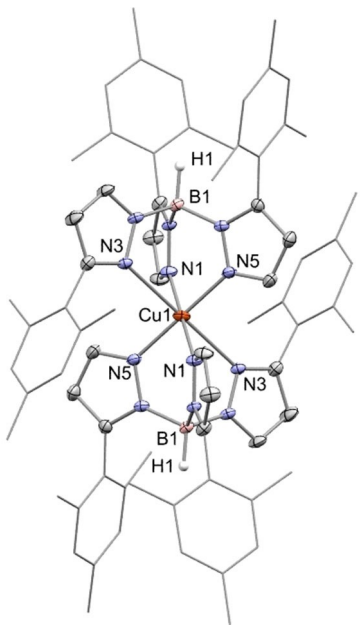

Figure 7. Molecular structure as determined by single crystal X-ray diffraction of $[(Tp^{H,Mes*})_2Cu]$, **4**·2MeCN, selected bond length (in Å) and angles (in °): Cu1-N1 = 1.996(3), Cu1-N3 = 2.565(3), Cu1-N5 = 1.979(3), N1-Cu1-N1 = 180.0, N5-Cu–N5 = 180.0; hydrogen atoms except for the ones bound to boron atoms omitted for clarity.

here, the two respective isomers of copper complexes could both be isolated and structurally characterized.

Solution state Properties

Heteroleptic Complexes

^{1}H NMR spectroscopic investigations with complexes **2-a** and **2-e** were not successful, which is understandable, as the reciprocal longitudinal relaxation times T_{1e}^{-1} of Mn^{2+} and Cu^{2+} ions ($\approx 10^8\ s^{-1}$) are close to the scalar coupling constant of metal and proton (A/h $\approx 10^6\ s^{-1}$). Extensive line broadening is the result and detection and interpretation of NMR spectra can be challenging.[62–65] Since T_{1e}^{-1} is much larger for high spin Fe^{2+}, Co^{2+} and Ni^{2+} ions (10^{11}–$10^{12}\ s^{-1}$) than A/h, paramagnetically shifted but well resolved NMR spectra are accessible. The ^{1}H NMR spectra of the high-spin Fe^{2+}, Co^{2+} and Ni^{2+} complexes **2-b**, **2-c** and **2-d** could therefore be interpreted, and as expected they showed twelve paramagnetically shifted and broad resonances between 60 and −30 ppm, when $CDCl_3$ was used as the solvent. After addition of CD_3CN to the NMR solutions the range of signal increased (80 to −80 ppm) and an additional resonance could be noted, close to the residual proton signal of CD_3CN at 1.94 ppm. The latter was thus assigned to coordinated acetonitrile. None of the previously observed signals remained at the same position (Figure S21, Figure S24, Figure S27). This confirms the coordination of MeCN not only in the solid state, but also quantitatively in solution. Dissolved in $CDCl_3$ the diamagnetic zinc complex **2-f** also shows twelve well resolved resonances in the ^{1}H NMR spectrum, which are well in line with those reported in the literature.[47] A complete assignment of the resonances was reached by 2D NMR experiments revealing two inequivalent *ortho* methyl groups for the mesityl residues in the 3-position, which indicates a rigid orientation of these residues without fast rotation around the C–C bond on NMR timescale. In the case of **2-f**, CD_3CN addition caused only minor changes for the chemical shifts, due to the changed polarity of the solvent mixture. The abovementioned inequivalent *ortho* methyl groups now give rise to only one NMR resonance indicating a more dynamic behavior of the molecule. No additional resonance for coordinated acetonitrile could be identified (Figure S30).

As expected, complexes **2-a** and **2-f** are colorless in solution since d-d transitions are spin forbidden in high-spin d^5 systems and impossible in d^{10} systems. In contrast, complexes **2-c**, **2-d** and **2-e** are colored and show distinct absorption bands in the UV-vis spectra, which were recorded in dichloromethane (DCM). Aided by previous literature, the spectra of **2-c** and **2-d** in DCM could be fully assigned (see below).[3,66] Subsequently, MeCN was titrated into the solutions (Figure 8). In case of the cobalt complex, this led to a color change from blue to purple, which is accompanied by a decrease of the intensities of a broad triplet band between 550 and 700 nm (ε_{max}(654 nm) = 495 L mol^{-1} cm^{-1}, $^4A_2 \rightarrow {}^4T_1(P)$) and of a broad and weaker absorption band at 850 nm (ε_{max} = 35 L mol^{-1} cm^{-1}, $^4A_2 \rightarrow {}^4T_1(F)$). The doublet of the $^4A_2 \rightarrow {}^4T_2(F)$ transition should be found well out of the measured range (2000–4000 nm). Concomitantly, the absorption intensity of the $\pi \rightarrow \pi^*$ transition in the UV region around 300 nm increases. Furthermore, a band at 467 nm (ε_{max} = 69 L mol^{-1} cm^{-1}) appears (Figure 8a). The nickel complex

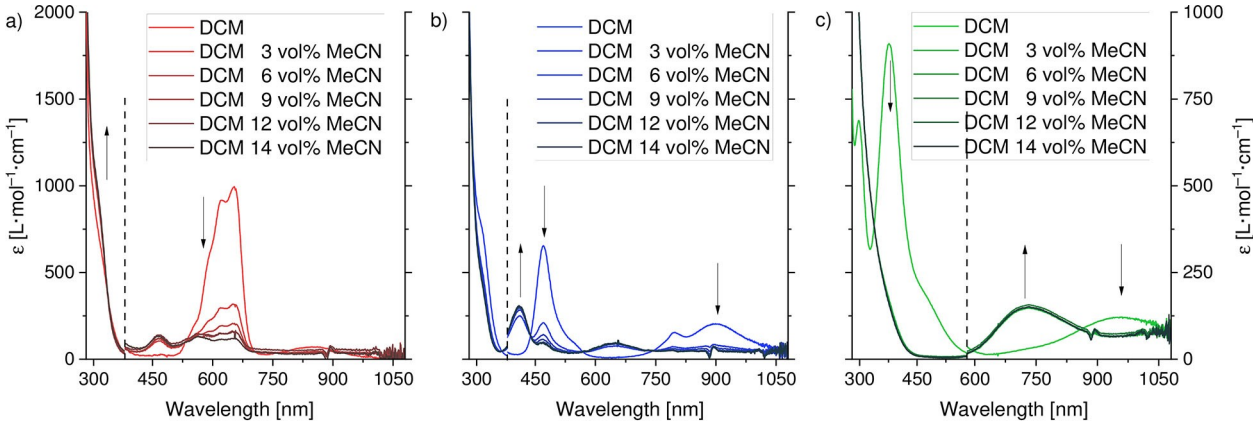

Figure 8. Electronic spectra of a) [Tp^{Me,Hs}*CoCl], **2-c**, (red), b) [Tp^{Mes,H}*NiCl], **2-d**, (blue) and c) [Tp^{Mes,H}*CuCl], **2-e**, (green) in DCM (0.4 mmol/L). Titration experiments with increasing volume ratios of MeCN to give [Tp^{Mes,H}*Co(NCMe)Cl], **2-c(MeCN)**, (dark red) b) [Tp^{Mes,H}*Ni(NCMe)Cl], **2-d(MeCN)**, (dark blue) and c) [Tp^{Mes,H}*Cu(NCMe)Cl], **2-e(MeCN)**, (dark green)); volume changes due to MeCN addition were considered for the calculation of the extinction coefficient ε.

changes color from orange to green and at the same time in the electronic spectrum the bands at 470 nm (ε_{max} = 327 L mol^{-1} cm^{-1}, $^3T_1 \rightarrow {}^3A_2(F)$) with a shoulder at around 540 nm ($^3T_1 \rightarrow {}^3T_1(P)$), at 796 nm ($\varepsilon_{max}$ = 79 L mol^{-1} cm^{-1}, $^3T_1 \rightarrow {}^3T_1(P)$) and at 900 nm ($\varepsilon_{max}$ = 101 L mol^{-1} cm^{-1}, $^3T_1 \rightarrow {}^3T_2(F)$) decrease in intensity, while absorption bands at 410 and 650 nm (ε_{max} = 154, 48 L mol^{-1} cm^{-1}) evolve (Figure 8b). In the UV region, a similar increase of absorption bands can be observed as described for the cobalt complex. For copper(II) only one d-d transition ($^2T_2 \rightarrow {}^2E(D)$) is expected, but as observed for the cobalt(II) and nickel(II) complexes a splitting of the bands can occur due to reduced symmetry by inequality of nitrogen and chlorido ligands. Complex **2-e** changes color with addition of MeCN from ochre to green, which goes along with an almost complete disappearance of previously intense bands at 298 and 377 nm (ε_{max} = 1377, 1817 L mol^{-1} cm^{-1}) as well as a broad band at 960 nm (ε_{max} = 123 L mol^{-1} cm^{-1}). Again, the absorption in the UV region increases as well as the intensity of a weak band at 730 nm (ε_{max} = 154 L mol^{-1} cm^{-1}) (Figure 8c).

Altogether, the change from fourfold to fivefold coordination in the course of the binding of MeCN induces a hypsochromic shift evident by clearly visible color changes as a result of larger ligand field splitting and d-d transitions of higher energy.

Homoleptic Complexes

The diamagnetic complex **3-f** showed a well resolved ^{1}H NMR spectrum. Based on the molecular structure of complex **3-f** determined by single crystal X-ray diffraction, a rather complicated ^{1}H NMR spectrum had been expected, as all three pyrazolyl groups and all three mesityl groups of each coordinating Tp ligand are chemically inequivalent and individual resonances for *ortho* methyl groups of each mesityl residue, as seen for the heteroleptic complex **2-f**, could be anticipated, too. Surprisingly, the ^{1}H NMR spectrum of **3-f** showed only one set of signals for the pyrazolyl donors with the mesityl residue in the 3-position and one set for the pyrazolyl donors with the mesityl residue in the 5-position in a ratio of 2:1 (Figure S35). Fast (on the NMR time scale) dynamic processes are a convincing explanation for this spectrum (Scheme 4). Similar observations had been made before for [(κ^2-Tp^{Ph,H})$_2$Zn], **IV-f**, where all pyrazolyl donors gave identical ^{1}H NMR resonances.[11,29]

For the reasons given above (unfavorable T_{1e}^{-1}), the ^{1}H NMR spectra recorded for **3-a** and **3-e**, like those of **2-a** and **2-e**, were uninterpretable. However, in contrast to the corresponding heteroleptic complexes, this was true also for **3-b**, **3-c** and **3-d**. Fast dynamic processes as discussed above for the zinc complex may also explain this finding, as it could lead to a further broadening of the paramagnetic NMR resonances to an extent that no resolution of spectra is possible.

A Mössbauer spectrum recorded for a frozen solution (THF) of **3-b** exhibited a doublet with a similar isomer shift and quadrupole splitting (δ = 1.09 mm/s, ΔE_q = 3.80 mm/s, see Figure S38) as observed for the solid sample, which is a good indication that the fivefold coordination observed for the solid sample is retained in solution, at least at low temperatures.

The position and the extinction coefficients of absorption bands in the electronic spectra of complexes **3-c** and **3-d** at

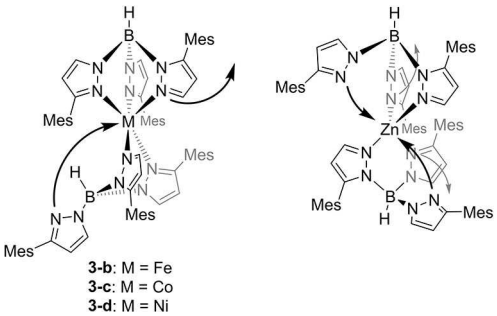

Scheme 4. Proposed dynamic processes in solution for the homoleptic complexes based on the results of ^{1}H NMR and UV-vis spectroscopy.

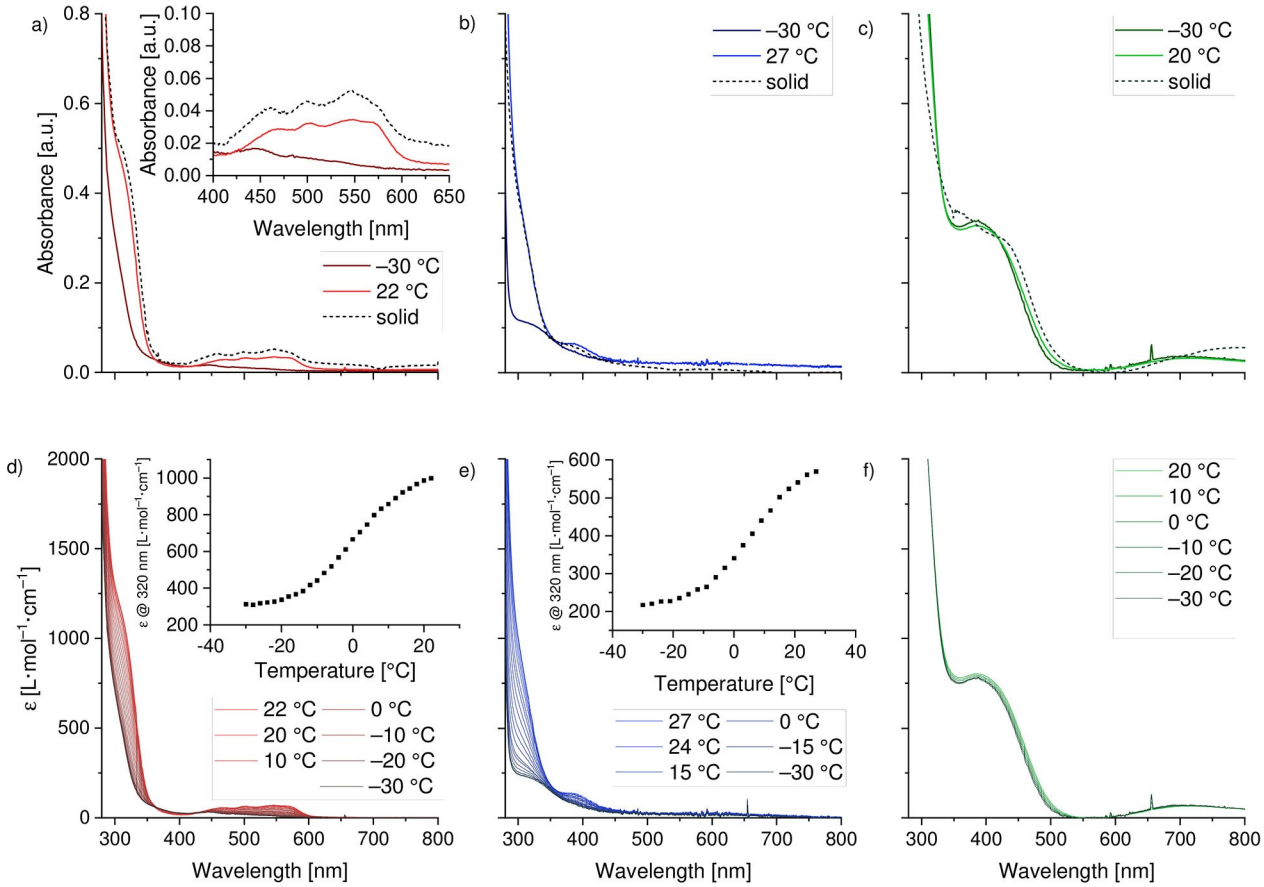

Figure 9. Electronic spectra recorded for a) $[(Tp^{Mes,H*})_2Co]$, **3-c**, (red), b) $[(Tp^{Mes,H*})_2Ni]$, **3-d**, (blue), and c) $[(Tp^{Mes,H*})_2Cu]$, **3-e**, (green) at ambient and low temperatures (DCM, 0.4 mmol/L, solid lines) as well as for the solid state (KBr pellet, dashed line) and d), e), f) thermochromic behavior of the complexes in solution (DCM, 0.4 mmol/L); insets show the decrease of the absorbance at 320 nm with decreasing temperature; volume changes due to temperature variation were considered for the calculation of the extinction coefficient ε.

ambient temperature resemble well the ones observed for **2-c (MeCN)** and **2-d(MeCN)**. As one should expect, the absorption pattern of complex **3-e** resembles much better the one observed for the tetrahedral complex **2-e**, in terms of the position of the absorption bands, than the one of **2-e(MeCN)** but a significant broadening of the band at 390 nm can be observed.

In all three cases, the electronic spectra at ambient temperatures in solution agree nicely with the spectra of the solid samples, disregarding the absolute intensity of the absorptions. This indicates that the coordination observed in the solid state is mostly retained in solution at ambient temperature for **3-c**, **3-d** and **3-e**.

The cobalt(II) and nickel(II) complexes **3-c** and **3-d** show thermochromism in solution (Figure 9) but not in solid state. With decreasing temperature, in the UV-vis spectrum of a solution of **3-c** a decrease of the absorptions at 320 ($\pi\rightarrow\pi^*$) and between 400 and 600 nm ($\varepsilon_{max}(547\ nm) = 70\ L\,mol^{-1}\,cm^{-1}$, d-d transition) could be observed, accompanied with a decrease of the color intensity of the complex solution. Similar observations were made for the nickel complex **3-d**, which showed intensity decreases of the band in the UV region at 320 nm ($\pi\rightarrow\pi^*$) and of a weak band at 390 nm ($\varepsilon_{max} = 135\ L\,mol^{-1}\,cm^{-1}$, d-d transition), accompanied by a color change from light blue to almost colorless with decreasing temperature. The resulting extinction coefficients are well below $50\ L\,mol^{-1}\,cm^{-1}$ and indicate the formation of species with centrosymmetrically coordinated metal ions, where the rule of Laporte applies, that is, these findings point to a structure change at low temperatures. Similarly weak absorptions can be observed for the homoleptic complexes $[(Tp^{Ph,Me})_2M]$ (**V-c**: M = Co, **V-d**: M = Ni), which are characterized by octahedral coordination spheres (see Supporting Information for further details). However, due to the large steric demand of the mesityl residues, a regular octahedral coordination appears difficult to achieve for the homoleptic complexes under investigation here (see also discussion below).

To get more insights into the coordination behavior of the $Tp^{Mes,H*}$ ligand in combination with divalent transition metal ions, a series of DFT calculations was performed. The structures of complexes **3-b**, **3-c** and **3-d** were optimized with the B3LYP (Def2-SVP/-TZVP) functional/basis set in quintet (**3-b**), quartet (**3-c**) and triplet states (**3-d**) (see Supporting Information for further details).

As expected, the optimized structures resemble well the ones found experimentally (Figure 9, Figure S39, Figure S41).

The M···HB distances predicted by computation are almost similar for **3-b** and **3-c** and significantly shorter for **3-d** as it is also found for the experimentally determined structures (Table 4). In general, the computed M···HB distances are slightly shorter than found by X-ray diffraction analysis. The trend of the geometric indices matches well the experimental values. Only the computed τ_5 of **3-d** is significantly smaller than those found experimentally.

NBO analysis of the metal borohydride interaction revealed a stabilization by interaction of the filled H–B σ-MO to partly filled metal *d*-orbitals. Interestingly the stabilization is largest for the nickel(II) and smallest for the cobalt(II) complex. A similar stabilization was proposed based on NBO analysis for homoleptic bis(pyrazolyl-1-yl) copper(II) complexes.[67]

Having shown that the experimental structures can be nicely reproduced by the chosen theoretical method and bearing in mind the indications for structural flexibility, as discussed above, we were interested to test whether alternative structures are stable. To search for further local energy minima, for instance, **3-f** featuring a tetrahedrally coordinated metal center was used as a starting structure to optimise similar structures for iron(II), cobalt(II) and nickel(II). Indeed, this proved possible (Figure 10b, Figure S40, Figure S42), and the total energy of the three computed structures is only insignificantly higher compared to the pentagonal structures (Table 4). This confirms that indeed more than just one energetically accessible, local minimum exists on the potential energy surface of $[(Tp^{Mes*})_2M]$ complexes. Considering the thermochromic behavior of **3-c** and **3-d**, as outlined above, which suggests the existence of a stable centrosymmetric structure (where the rule of Laporte would apply), we also attempted the optimisation of structures with a six-fold coordination around the metal centers. The starting coordination geometry was similar to the distorted octahedral coordination found for complex **4** and optimization was performed after replacement of the Cu^{2+} ion by a Ni^{2+} ion and exchange of the $Tp^{H,Mes*}$ by $Tp^{Mes,H*}$ ligands. The optimization yielded neither a square planar nor a distorted octahedral coordination environment, but yet another pentagonal complex

Table 4. Selected results of DFT calculations with B3LYP(Def2-SVP/-TZVP) basis set: metal borohydride distances, geometric indices and energy difference between pentagonal and tetrahedral structures; experimental values in parentheses.

M		Structure	M···HB [Å]	τ_4[a][48] τ_5[b][49]	ΔE [kcal/mol]
Fe	**3-b**	pentagonal	2.246 (2.310)	0.38[b] (0.34)	
Co	**3-c**	pentagonal	2.236 (2.334)	0.39[b] (0.33)	
Ni	**3-d**	pentagonal	1.988 (2.195)	0.17[b] (0.28)	
Fe	**3-b**	tetrahedral	-	0.81[a]	+2.80
Co	**3-c**	tetrahedral	-	0.82[a]	+0.86
Ni	**3-d**	tetrahedral	-	0.78[a]	+5.31

[a] τ_4. [b] τ_5.

Table 5. Crystallographic data of the heteroleptic complexes **2-a(MeCN)**, **2-d(MeCN)**·MeCN, **2-e(MeCN)**·MeCN and **2-f**·2MeCN as well as of the homoleptic complexes **3-a**, **3-b**·0.5CH_2Cl_2, **3-c** and **3-d**.

	2-a(MeCN)	**2-d(MeCN)** ·MeCN	**2-e(MeCN)** ·MeCN	**2-f**·2MeCN	**3-a**	**3-b**·0.5C_2Cl_2	**3-c**	**3-d**
Formula	$C_{38}H_{43}BClMnN_7$	$C_{40}H_{46}BClNiN_8$	$C_{40}H_{46}BClCuN_8$	$C_{40}H_{46}BClZnN_8$	$C_{72}H_{80}B_2MnN_{12}$	$C_{72.5}H_{81}B_2ClMnN_{12}$	$C_{72}H_{80}B_2CoN_{12}$	$C_{72}H_{80}B_2NiN_{12}$
M_r/g·mol^{-1}	698.99	743.82	748.65	1209.33	1190.04	1233.41	1194.03	1193.81
Crystal system	Tetragonal	Triclinic	Triclinic	Triclinic	Monoclinic	Monoclinic	Monoclinic	Monoclinic
Crystal color/shape	colorless/ rod	blue/ block	blue/ fragment	colorless/ plate	colorless/ fragment	colorless/ block	pink/ fragment	blue/ fragment
SG	$I4_1cd$	*P*-1	*P*-1	*P*-1	$P2_1/c$	$P2_1/c$	$P2_1/c$	$P2_1/c$
a/Å	32.0179(10)	9.1548(6)	9.161(4)	9.2917(5)	19.0675(11)	11.9330(7)	11.9296(8)	11.8698(8)
b/Å	32.0179(10)	11.9729(8)	12.024(6)	11.2048(6)	22.3812(13)	18.2558(9)	18.2017(13)	18.1951(10)
c/Å	14.7769(4)	19.5177(13)	19.583(10)	19.5264(11)	15.5884(8)	31.9857(16)	31.985(2)	32.071(2)
α/°	90	102.025(2)	102.204(13)	91.186(2)	90	90	90	90
β/°	90	101.418(2)	101.219(13)	102.126(2)	102.140(2)	99.312(2)	98.913(2)	98.462(2)
γ/°	90	104.970(2)	105.669(12)	91.195(2)	90	90	90	90
V/Å^3	15148.5(10)	1948.3(2)	1956.1(17)	1986.48(19)	6503.6(6)	6876.1(6)	6861.4(8)	6851.0(7)
Z	16	2	2	2	4	4	4	4
Density/ g·cm^{-3}	1.226	1.268	1.271	1.255	1.215	1.191	1.156	1.157
F(000)	5872	784	786	788	2524	2612	2532	2536
Θ range ()°	2.55–25.37	2.35–25.38	2.36–25.37	2.24–25.41	2.37–25.43	2.23–25.39	2.23–25.47	2.23–25.17
Total nr. of refl.	47385	25162	72600	50425	113961	96416	110383	116907
Independent reflections	6941	7129	7157	7307	11965	12644	12699	12231
Refl. with $I > 2\sigma(I)$	6074	5929	6179	6704	10285	9966	10611	9818
R_{int}	0.0680	0.0410	0.0508	0.0341	0.0459	0.0774	0.0614	0.0779
R indices [$I > 2\sigma(I)$]	$R_1 = 0.0325$ $wR_2 = 0.0694$	$R_1 = 0.0356$ $wR_2 = 0.0794$	$R_1 = 0.0327$ $wR_2 = 0.0758$	$R_1 = 0.0282$ $wR_2 = 0.0729$	$R_1 = 0.0372$ $wR_2 = 0.0926$	$R_1 = 0.0714$ $wR_2 = 0.1926$	$R_1 = 0.0450$ $wR_2 = 0.1022$	$R_1 = 0.0538$ $wR_2 = 0.1040$
R indices (all data)	$R_1 = 0.0440$ $wR_2 = 0.0746$	$R_1 = 0.0497$ $wR_2 = 0.0851$	$R_1 = 0.0427$ $wR_2 = 0.0801$	$R_1 = 0.0322$ $wR_2 = 0.0749$	$R_1 = 0.0461$ $wR_2 = 0.0989$	$R_1 = 0.0919$ $wR_2 = 0.2092$	$R_1 = 0.0580$ $wR_2 = 0.1076$	$R_1 = 0.0762$ $wR_2 = 0.1113$
GooF (all data)	1.029	1.001	1.051	1.011	1.035	1.025	1.053	1.077
Completeness to 25°	0.999	0.998	0.999	0.998	0.999	0.999	0.999	0.996
Largest diff. peak and hole	−0.25/-0.24	−0.35/+0.28	−0.45/+0.30	−0.33/+1.05	−0.35/+0.37	−1.24/+2.25	−0.41/+0.52	−0.39/ +0.33

Table 6. Crystallographic data of the homoleptic complexes **3-e**·$2CH_2Cl_2$, **3-f** and **4**·2MeCN.

	3-e·$2CH_2Cl_2$	**3-f**	**4**·2MeCN
Formula	$C_{74}H_{84}B_2Cl_4CuN_{12}$	$C_{72}H_{80}B_2ZnN_{12}$	$C_{76}H_{86}B_2CuN_{14}$
M_r/g mol^{-1}	1368.49	1200.47	1280.74
Crystal system	Triclinic	Monoclinic	Monoclinic
Crystal color/ shape	green/block	colorless/ block	colorless/elongated plate
SG	*P*-1	*C*2/c	$P2_1/n$
a/Å	11.3010(8)	25.705(5)	15.9096(9)
b/Å	12.2480(9)	11.125(2)	12.8162(8)
c/Å	27.026(2)	26.219(4)	17.0936(10)
α/°	79.890(2)	90	90
β/°	84.212(2)	114.358(7)	96.048(2)
γ/°	72.907(2)	90	90
V/Å^3	3515.2(4)	6830(2)	3466.0(4)
Z	2	4	2
Density/ g cm^{-3}	1.293	1.167	1.227
F(000)	1438	2544	1358
Θ range ()°	2.19–25.19	2.33-25.08	2.30–25.42
Total nr. of refl.	110895	16468	149906
Independent reflections	12611	5950	6382
Refl. with $I > 2\sigma(I)$	10380	4627	5687
R_{int}	0.0589	0.0870	0.0795
R indices [$I > 2\sigma(I)$]	$R_1 = 0.0484$ $wR_2 = 0.1219$	$R_1 = 0.0840$ $wR_2 = 0.2215$	$R_1 = 0.0706$ $wR_2 = 0.1805$
R indices (all data)	$R_1 = 0.0632$ $wR_2 = 0.1305$	$R_1 = 0.1015$ $wR_2 = 0.2308$	$R_1 = 0.0798$ $wR_2 = 0.1850$
GooF (all data)	1.020	1.077	1.203
Completeness to 25°	0.999	0.984	0.998
Largest diff. peak and hole	−1.34/+0.78	−0.84/+2.09	−63/+0.47

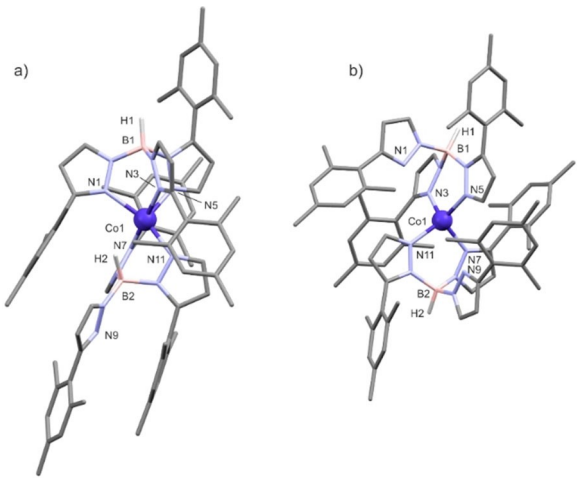

Figure 10. Optimized (B3LYP(Def2-SVP/-TZVP)) molecular structures of **3-c** in its quartet state (a) [(κ^2-$Tp^{Mes,H*}$)(κ^3-$Tp^{Mes,H*}$)Co] with a five-fold coordinated Co atom and (b) [(κ^2-$Tp^{Mes,H*}$)$_2$Co] with tetrahedral coordination; selected bond length (in Å) and angles (in °): a) Co1-N1 = 2.121, Co1-N3 = 2.2383, Co1-N5 = 2.018, Co1-N7 = 2.130, Co1-N11 = 2.073, Co1-H2 = 2.236, N1-Co1-N11 = 155.45, N3-Co1-N7 = 179.34; b) Co1-N3 = 2.019, Co1-N5 = 1.986, Co1-N7 = 1.986, Co1-N11 = 2.019, N5-Co1-N11 = 131.23, N3-Co1-N7 = 113.61, hydrogen atoms except for the ones bound to boron atoms were omitted for clarity.

(Figure S43). A complex with all pyrazolyl donors binding did not emerge, but this may be a result of the limitations of the method or the chosen starting geometry.

Conclusion

The coordination behavior of a Tp ligand that so far has been underrepresented in the rich chemistry of Tp metal complexes, namely $Tp^{Mes,H*}$ (bis(3-mesitylpyrazol-1-yl)(5-mesitylpyrazol-1-yl) hydroborate), has been explored. This has provided useful information about the steric conditions it requires and brings about. It also led to the discovery of new structural motifs. Heteroleptic compounds of the type [$Tp^{Mes,H*}$MCl] readily bind acetonitrile molecules, both in the solid state and in solution, to give complexes [$Tp^{Mes,H*}$M(NCMe)Cl]. With regards to the homoleptic complexes, Tp_2M, for M = Mn, Fe, Co and Ni rare examples are reported, where two equal Tp ligands are bound to one metal center in differing ways, namely one in an κ^2 and one in an κ^3 mode. For the case of copper, a κ^2, κ^2 coordination was observed and ultrasound treatment during the synthesis was found to lead to a 1,2-borotropic rearrangement. Thus, a ligand formed, where now two mesityl residues are found in the 5-position of the Tp ligand. The corresponding copper complex is an isomer of [$(Tp^{Mes,H*})_2$Cu], being linked to it through a ligand rearrangement, and in fact there is no other precedence in the literature, where similarly two such isomers could both be isolated and structurally characterized. All compounds were found to be dynamic in solution and the cobalt(II) and nickel(II) complexes show thermochromism in solution, which has its origin in a structure change as suggested by their electronic spectra.

Experimental Section

General procedures: All experiments were carried out in a dry argon or nitrogen atmosphere using an MBraun glovebox, GS Glovebox Systemtechnik glovebox and/or standard Schlenk techniques. Solvents were purified employing an MBraun Solvent Purification System SPS. All materials were obtained from commercial vendors as ACS reagent-grade or better and used as received. Effective magnetic moments were determined by a magnetic susceptibility balance MSB-1 by Alpha (A Johnson Matthey Company). ATR-IR spectra of solid samples were recorded with a Bruker alpha FTIR spectrometer in the region 4000–400 cm^{-1}. Microanalyses were performed with a HEKAtech Euro EA 3000 elemental analyzer (we have frequently experienced that Tp complexes lead to C analyses, which are a little bit too low, while the results for the other elements fit).[68] UV-vis spectra were obtained at variable temperatures with an Agilent 8453 UV-vis spectrophotometer equipped with a Unisoku USP-203-A cryostat. SUPRASIL Quartz cells from Hellma Analytics with a 10 mm path length were used. Solid state UV-vis spectra were recorded of the samples as KBr pellets with a Cary 100 UV-vis spectrometer by Agilent. Mössbauer spectra were recorded with a SeeCo MS6 spectrometer and a Janis CCS-850 cryostat wit CTI-Cryogenics 8200 helium compressor. The temperature was controlled with a Lake-Shore 335 thermocontrol. The ligand K[$Tp^{Mes,H*}$], **1**, was synthesized as described by Trofimenko and coworkers from 3-mesityl pyrazole and potassium borohydride in comparable yield.[47] The separation

from K[Tp^{Mes,H}] was performed by fractionalized crystallization from cold acetonitrile. The preparation and full characterization of complexes **V-c**[45] and **V-d**[46] is described elsewhere. Only additional electronic spectra are provided herein (see Supporting Information).

Synthesis of [Tp^{Mes,H}*MnCl], 2-a, [Tp^{Mes,H}*CoCl] 2-c and [Tp^{Mes,H}*NiCl] 2-d: The synthesis followed the procedure published for complex **2-c**.[26] Potassium bis(3-mesitylpyrazol-1-yl)(5-mesitylpyrazol-1-yl) hydroborate (**1**) (607 mg, 1.00 mmol) was dissolved in DCM (12 mL). Manganese(II) chloride tetrahydrate (218 mg, 1.10 mmol), cobalt(II) chloride hexahydrate (262 mg, 1.10 mmol) or nickel(II) chloride hexahydrate (261 mg, 1.10 mmol), respectively, were dissolved in MeOH (12 mL). The potassium salt of the ligand in DCM was slowly added to the dissolved metal salt. The solution was stirred overnight. Subsequently, the reaction mixture was washed with brine (50 mL) and water (50 mL). The combined aqueous phases were extracted with DCM (30 mL) and the combined organic layers dried over Na_2SO_4. All volatiles were removed in *vacuo* and the resulting colorless (**2-a**), blue (**2-c**) or green (**2-d**) product freeze-dried from benzene. **2-a** was washed with MeOH (10 mL) and **2-c** was washed with MeCN (1×20 mL, 1× 8 mL) and dried in *vacuo* overnight. **2-a**: Yield: 326 mg (0.495 mmol, 50%), Elemental analysis: Calculated for $C_{36}H_{40}BClMnN_6$ (*MW* = 657.96 g/mol) C: 65.72 H: 6.13 N: 12.77 Found C: 64.86, H: 6.32, N: 12.40, concerning C deviation, see general procedures above; ATR-IR (solid): ν(B–H) 2489 cm^{-1}. **2-c**: Yield = 533 mg (0.81 mmol, 81%); Calculated for $C_{36}H_{40}BClCoN_6$ (*MW* = 661.95 g/mol) C: 65.32, H: 6.09, N: 12.70 Found C: 64.56, H: 6.16, N: 12.66, concerning C deviation, see general procedures above; ATR-IR (solid): 2517 [ν(B–H)] cm^{-1}; ^{1}H NMR (300 MHz, $CDCl_3$): $\delta = -5.42, -2.32, -0.83, 0.11, 0.47, 2.08, 4.60, 5.68, 42.64, 47.82, 56.88, 76.69$ ppm; ^{1}H NMR (300 MHz, $CDCl_3$/CD_3CN): $\delta = -61.26, -54.74, -23.76, -11.07, -1.15, 0.15, 1.96, 3.24, 13.13, 31.70, 61.92, 71.87, 80.80$ ppm. **2-d**: Yield: 85.6 mg (0.129 mmol, 30%), Elemental analysis: Calculated for $C_{36}H_{40}BClNiN_6$ (*MW* = 661.71 g/mol) C: 64.87 H: 6.05 N: 12.61 Found C:65.01, H: 6.09, N: 12.70; ATR-IR (solid): ν(B–H) 2518 cm^{-1}; ^{1}H NMR (300 MHz, $CDCl_3$): $\delta = -13.36, 2.10, 2.59, 3.13, 4.67, 5.92, 6.28, 6.45, 7.70, 25.15, 73.37, 76.96$ ppm; ^{1}H NMR (300 MHz, $CDCl_3$/CD_3CN): $\delta = 11.38, 1.30, 1.89, 2.80, 3.52, 4.72, 5.52, 7.80, 8.44, 36.15, 46.04, 61.92, 65.63$ ppm.

Synthesis of complex [Tp^{Mes,H}*FeCl], 2-b, and [Tp^{Mes,H}*CuCl], 2-e: The synthesis followed the procedure published for complex [Tp^{Mes,H}*FeCl], **2-b**.[26] Potassium bis(3-mesitylpyrazol-1-yl)(5-mesitylpyrazol-1-yl) hydroborate (**1**) (182 mg, 0.30 mmol) was dissolved in dichloromethane (12 mL). Iron(II) chloride (38 mg, 0.30 mmol) or copper(II) chloride (40 mg, 0.30 mmol), respectively, were dispersed in MeCN (12 mL). The potassium salt of the ligand in DCM was slowly added to the dispersion of the metal salt. The reaction mixture was stirred overnight. Subsequently, all volatiles were removed in *vacuo* and the resulting solid extracted with DCM (15 mL). MeCN (15 mL) was added and the solution reduced in *vacuo* to 3 mL. After filtration a colorless solid (**2-b**) or an ochre solid (**2-e**) was obtained which were dried in *vacuo*. **2-b**: Yield = 167 mg (0.253 mmol, 84%); Elemental analysis: Calculated for $C_{36}H_{40}BClFeN_6$ (*MW* = 658.86 g/mol) C: 65.63, H: 6.12, N: 12.76 Found C: 62.98, H: 6.20, N: 12.24, concerning C deviation, see general procedures above; ATR-IR (solid): 2517 [ν(B–H)] cm^{-1}; ^{1}H NMR (300 MHz, $CDCl_3$): $\delta = -27.18, -3.03, -0.31, 1.72, 2.24, 3.81, 4.96, 5.65, 11.71, 39.64, 57.32, 60.61$ ppm; ^{1}H NMR (300 MHz, $CDCl_3$/CD_3CN):

$\delta = -42.21, 14.42, -10.55, -9.15, -4.21, 1.31, 1.92, 2.62, 4.12, 22.79, 25.80, 54.79, 60.45$ ppm. **2-e**: Yield: 119 mg (0.179 mmol, 60%), Elemental analysis: Calculated for $C_{36}H_{40}BClCuN_6$ (*MW* = 666.56 g/mol) C: 64.87 H: 6.05 N: 12.61 Found C: 64.08, H: 6.16, N: 13.08, concerning C deviation, see general procedures above; ATR-IR (solid): ν(B–H) 2517 cm^{-1}.

Synthesis of [Tp^{Mes,H}*ZnCl] 2-f: Complex **2-f** was first prepared by Trofimenko and coworkers *via* a salt metathesis reaction of thallium bis(3-mesitylpyrazol-1-yl)(5-mesitylpyrazol-1-yl) hydroborate and zinc(II) chloride.[47] We found that it can be prepared alternatively starting from potassium bis(3-mesitylpyrazol-1-yl)(5-mesitylpyrazol-1-yl) hydroborate (**1**) (121 mg, 0.20 mmol), which was dissolved in DCM (2.8 mL). Zinc(II) chloride (27 mg, 0.20 mmol) was dissolved in MeOH (2.4 mL). The potassium salt of the ligand in DCM was slowly added to the dissolved metal salt. The solution was stirred overnight. The next day, the colorless solution was washed with brine (10 mL) and water (10 mL). The aqueous phase was extracted with DCM (6 mL) and the combined organic layers dried over Na_2SO_4. All volatiles were removed in *vacuo* and the obtained product freeze-dried from a benzene solution. The product was washed with MeCN (1×4 mL, 1×1.2 mL) and dried in *vacuo* overnight. Yield: 134 mg (0.124 mmol, 62%), ATR-IR (solid): ν(B–H) 2518 cm^{-1}, ^{1}H NMR (300 MHz, $CDCl_3$): $\delta = 1.87$ (s, 6H, *o*-Mes*CH_3), 1.93 (s, 6H, *o*-MesCH_3), 1.95 (s, 6H, *o*-MesCH_3), 2.29 (s, 6H, *p*-MesCH_3), 2.42 (s, 3H, *p*-Mes*CH_3), 4.07 (s, br, 1H, B*H*), 6.11 (m, 3H, 4-PzH, 4-Pz**H*), 6.88 (s, 2H, *m*-Mes*H*), 6.90 (s, 2H, *m*-Mes*H*), 7.02 (s, 2H, *m*-Mes**H*), 7.63 (d, $J = 2.2$ Hz, 2H, 5-Pz*H*), 7.71 (d, $J = 2.0$ Hz, 1H, 3-Pz**H*) ppm; ^{1}H NMR (300 MHz, $CDCl_3$/CD_3CN): $\delta = 1.81$ (s, 6H, *o*-Mes*CH_3), 1.87 (s, 12H, *o*-MesCH_3), 2.24 (s, 6H, *p*-MesCH_3), 2.36 (s, 3H, *p*-Mes*CH_3), 4.03 (s, br, 1H, B*H*), 6.08 (m, 3H, 4-PzH, 4-Pz**H*), 6.83 (s, 2H, *m*-Mes*H*), 6.84 (s, 2H, *m*-Mes*H*), 6.97 (s, 2H, *m*-Mes**H*), 7.61 (d, $J = 2.4$ Hz, 2H, 5-Pz*H*), 7.66 (d, $J = 1.9$ Hz, 1H, 3-Pz**H*) ppm; Mes* refers to the mesityl group in 5-postion of the pyrazolyl group, Pz* refers to the pyrazolyl group with mesityl group in 5-position, all other analytical data fit to the literature values.[47]

Synthesis of [(Tp^{Mes,H}*)$_2$Mn] 3-a, [(Tp^{Mes,H}*)$_2$Fe] 3-b and [(Tp^{Mes,H}*)$_2$Zn] 3-f: Potassium bis(3-mesitylpyrazolyl)-5-mesitylpyrazolyl hydroborate (**1**) (364 mg, 0.60 mmol) and manganese(II) chloride (38 mg, 0.30 mmol), iron(II) chloride (38 mg, 0.30 mmol) or zinc(II) chloride (41 mg, 0.30 mmol), respectively, were dispersed in THF (30 mL). The reaction mixture was kept in an ultrasonic bath (45 min). After the reactions had reached completion all volatiles were removed in *vacuo* and the residue extracted with DCM (15 mL). MeCN (15 mL) was added and the resulting solution reduced in *vacuo* to 3 mL. After filtration, a colorless solid (**3-a**, **3-b** or **3-f**) was obtained which was dried in *vacuo*. The filtrate was cooled to −30 °C to isolate a second crop. **3-a**: Yield: 281 mg (0.236 mmol, 79%), Elemental analysis: Calculated for $C_{72}H_{80}B_2MnN_{12}$ (*MW* = 1190.07 g/mol) C: 72.67 H: 6.78 N: 14.12 Found C: 72.02, H: 6.84, N: 13.89; ATR-IR (solid): ν(B–H) 2489 cm^{-1}. **3-b**: Yield: 274 mg (0.230 mmol, 77%), Elemental analysis: Calculated for $C_{72}H_{80}B_2FeN_{12}{\cdot}CH_2Cl_2$ (*MW* = 1275.91 g/mol) C: 68.72 H: 6.48 N: 13.17 Found C: 68.67, H: 6.97, N: 12.70; ATR-IR (solid): ν(B–H) 2480 cm^{-1}. **3-f**: Yield: 198 mg (0.165 mmol, 55%), Elemental analysis: Calculated for $C_{72}H_{80}B_2ZnN_{12}{\cdot}CH_2Cl_2$ (*MW* = 1285.44 g/mol) C: 68.21 H: 6.43 N: 13.08 Found C: 68.62, H: 6.72, N: 13.11; ATR-IR (solid): ν(B − H) 2482 cm^{-1}; ^{1}H NMR (300 MHz, $CDCl_3$): $\delta = 1.57$ (s, 12H, *o*-Mes*CH_3), 1.69 (s, 24H, *o*-MesCH_3), 2.19 (s, 12H, *p*-MesCH_3), 2.34 (s, 6H, *p*-Mes*CH_3), 4.06 (s, br, 2H, B*H*), 5.43 (d, $J = 2.0$ Hz, 2H, 4-Pz**H*), 5.93 (d, $J = 2.1$ Hz, 4H, 4-Pz*H*), 6.67 (s, 8H, *m*-Mes*H*), 6.87 (s, 4H, *m*-Mes**H*), 7.38 (d, $J = 2.1$ Hz, 4H, 5-Pz*H*), 7.82 (d, $J = 2.0$ Hz, 2H, 3-Pz**H*) ppm; Mes* refers to the mesityl group in 5-postion of the pyrazolyl group, Pz* refers to the pyrazolyl group with mesityl group in 5-position.

Synthesis of [(Tp^{Mes,H}*)$_2$Co] 3-c: Potassium bis(3-mesitylpyrazolyl)-5-mesitylpyrazolyl hydroborate (**1**) (364 mg, 0.60 mmol) and cobalt(II) chloride (38 mg, 0.30 mmol) were dispersed in THF (30 mL). The reaction mixture was treated in an ultrasonic bath (90 min). After complete reaction, the solution was filtered, all volatiles of the filtrate were removed in *vacuo* and the residue extracted with DCM (15 mL). MeCN (15 mL) was added and the solution reduced in

vacuo to 3 mL. After filtration a lilac solid (**3-c**) was obtained which was dried in *vacuo*. The filtrate was reduced to 1 mL and cooled to −30 °C to isolate a second crop.

Yield: 262 mg (0.219 mmol, 73 %), Elemental analysis: Calculated for $C_{72}H_{80}B_2CoN_{12}\cdot CH_2Cl_2$ (*MW* = 1297.01 g/mol) C: 68.55, H: 6.46, N: 13.14 Found C: 68.97, H: 7.12, N: 12.49; ATR-IR (solid): ν(B − H) 2481 cm^{-1}.

Synthesis of [(Tp^{Mes,H*})$_2$Ni] 3-d: Potassium bis(3-mesitylpyrazolyl)-5-mesitylpyrazolyl hydroborate (**1**) (364 mg, 0.60 mmol) and (93 mg, 0.30 mmol) were dispersed in THF (30 mL) and stirred at room temperature (10 min). The reaction mixture was treated in an ultrasonic bath (60 min). After complete reaction, the solution was filtered, all volatiles of the filtrate were removed in *vacuo* and the residue extracted with DCM (15 mL). MeCN (15 mL) was added and the solution reduced in *vacuo* to 3 mL. After filtration and repeated washing with MeCN a light blue solid (**3-d**) was obtained which was dried in *vacuo*. The filtrate was cooled to −30 °C to isolate a second crop.

Yield: 254 mg (0.213 mmol, 71 %), Elemental analysis: Calculated for $C_{72}H_{80}B_2NiN_{12}$ (*MW* = 1193.83 g/mol) C: 72.44 H: 6.75 N: 14.08 Found C: 72.03, H: 6.81, N: 13.87; ATR-IR (solid): ν(B–H) 2485 cm^{-1}.

Synthesis of [(Tp^{Mes,H*})$_2$Cu] 3-e

Potassium bis(3-mesitylpyrazolyl)-5-mesitylpyrazolylhydroborate (**1**) (364 mg, 0.60 mmol) and copper(II) chloride (40.3 mg, 0.30 mmol) were dispersed in THF (30 mL) and stirred overnight. After complete reaction, all volatiles were removed in *vacuo* and the green residue extracted with DCM (15 mL). MeCN (15 mL) was added and the solution reduced in *vacuo* to 3 mL. After filtration, a green solid (**3-e**) was obtained which was dried in *vacuo*.

Yield: 219 mg (0.180 mmol, 60 %), Elemental analysis: Calculated for $C_{72}H_{80}B_2CuN_{12}$ (*MW* = 1198.68 g/mol) C: 72.15 H: 6.73 N: 14.02 Found C: 69.41, H: 6.71, N: 13.70, concerning C deviation, see general procedures above; ATR-IR (solid): ν(B − H) 2451 cm^{-1}.

Single Crystal X-ray Crystallography: The data collections (Table 5 and 6) were performed with a Bruker D8 Venture area detector with Mo–Kα radiation (λ = 0.71073 Å). Multi-scan absorption corrections implemented in Sadabs[69] were applied to the data. The structures were solved by intrinsic phasing method (Shelxt-2014)[70] and refined by full matrix least square procedures based on F^2 with all measured reflections (Shelxl-2018)[71] with anisotropic temperature factors for all non-hydrogen atoms. All hydrogen atoms were added geometrically and refined by using a riding model except for the ones attached to the boron atoms which were found in the residual electron density map and freely refined. Squeeze was calculated with the Platon Program in structures of **3-c**·0.5CH_2Cl_2, **3-d** and **3-f**.[72]

Deposition Numbers 2012446 (for **2-a(MeCN)**), 2012437 (for **2-d(MeCN)**·MeCN), 2012436 (for **2-e(MeCN)**·MeCN), 2012443 (for **2-f**·2MeCN), 2012444 (for **3-a**), 2012438 (for **3-b**·0.5CH_2Cl_2), 2012439 (for **3-c**), 2012440 (for **3-d**), 2012445 (for **3-e**·2CH_2Cl_2), 2012441 (for **3-f**), and 2012442 (for **4**·2MeCN) contain the supplementary crystallographic data for this paper. These data are provided free of charge by the joint Cambridge Crystallographic Data Centre and Fachinformationszentrum Karlsruhe Access Structures service www.ccdc.cam.ac.uk/structures.

Single crystal suitable for structure determination by X-ray diffraction of complex **2-a(MeCN)** were grown from hot MeCN. Single crystals of **2-b(MeCN)**·MeCN, **2-c(MeCN)**·MeCN, **2-d(MeCN)**·MeCN, **2-e(MeCN)**·MeCN, **2-f**·2MeCN were obtained by layering a concentrated solution of **2-b**, **2-c**, **2-d**, **2-e** or **2-f**, respectively, in DCM with MeCN. Single crystals suitable for structure determination by X-ray diffraction of **3-a**, **3-b**·0.5CH_2Cl_2, **3-e**·2CH_2Cl_2, **3-f** and **4**·2MeCN were grown by layering a concentrated complex solution in DCM with MeCN and crystals of **3-c** and **3-d** were grown by layering a concentrated complex solution in THF with Et_2O. The crystallization attempt of **3-d** was cooled to −30 °C.

Acknowledgments

CL and LM are grateful to UniSysCat, as this work was funded by the Deutsche Forschungsgemeinschaft (DFG, German Research Foundation) under Germany's Excellence Strategy -EXC 2008/1 (UniSysCat) - 390540038. Support by the Humboldt-Universität zu Berlin is also gratefully acknowledged. Open access funding enabled and organized by Projekt DEAL.

Conflict of Interest

The authors declare no conflict of interest.

Keywords: Tris(pyrazolyl)borate · Ligand · Structure · rearrangement · First row metal

[1] S. Trofimenko, *J. Am. Chem. Soc.* **1966**, *88*, 1842–1844.
[2] N. Burzlaff, *Angew. Chem. Int. Ed.* **2009**, *48*, 5580–5582; *Angew. Chem.* **2009**, *121*, 5688–5690.
[3] J. Krzystek, D. C. Swenson, S. A. Zvyagin, D. Smirnov, A. Ozarowski, J. Telser, *J. Am. Chem. Soc.* **2010**, *132*, 5241–5253.
[4] M. Sallmann, C. Limberg, *Acc. Chem. Res.* **2015**, *48*, 2734–2743.
[5] S. Hoof, C. Limberg, *Inorg. Chem.* **2019**, *58*, 12843–12853.
[6] E. N. Mirts, A. Bhagi-Damodaran, Y. Lu, *Acc. Chem. Res.* **2019**, *52*, 935–944.
[7] W. Maret, B. L. Vallee, *Methods Enzymol.* **1993**, *226*, 52–71.
[8] K. Hakansson, A. Wehnert, A. Liljas, *Acta Crystallogr. Sect. D* **1994**, *50*, 93–100.
[9] F. X. Gomis-Ruth, F. Grams, I. Yiallouros, H. Nar, U. Kusthardt, R. Zwilling, W. Bode, W. Stocker, *J. Biol. Chem.* **1994**, *269*, 17111–17117.
[10] S. Trofimenko, J. R. Long, T. Nappier, S. G. Shore, in *Inorganic Synthesis 1939-, Vol. XII/3* (Ed.: R. W. Parry), McGraw-Hill Book Company, New York, **1970**, pp. 99–109.
[11] S. Trofimenko, *Chem. Rev.* **1972**, *72*, 497–509.
[12] A. Kremer-Aach, W. Kläui, R. Bell, A. Strerath, H. Wunderlich, D. Mootz, *Inorg. Chem.* **1997**, *36*, 1552–1563.
[13] L. R. Kadel, J. R. Bullinger, R. R. Baum, C. E. Moore, D. L. Tierney, D. M. Eichhorn, *Eur. J. Inorg. Chem.* **2016**, *2016*, 2543–2551.
[14] T. R. Belderraín, M. Paneque, E. Carmona, E. Gutiérrez-Puebla, M. A. Monge, C. Ruiz-Valero, *Inorg. Chem.* **2002**, *41*, 425–428.
[15] S. Trofimenko, J. C. Calabrese, J. S. Thompson, *Inorg. Chem.* **1987**, *26*, 1507–1514.
[16] P. Ghosh, J. B. Bonanno, G. Parkin, *Dalton Trans.* **1998**, *131*, 2779–2781.
[17] H. M. Echols, D. Dennis, *Acta Crystallogr. Sect. B* **1973**, *32*, 1627–1630.
[18] H. Kokusen, H. Hasegawa, *Dalton Trans.* **1996**, 195–201.
[19] H. V. R. Dias, J. D. Gorden, *Inorg. Chem.* **1996**, *35*, 318–324.
[20] T. Ruman, Z. Ciunik, A. Goclan, M. Lukasiewicz, S. Wolowiec, *Polyhedron* **2001**, *20*, 2965–2970.
[21] J. C. Calabrese, P. J. Domaille, J. S. Thompson, S. Trofimenko, *Inorg. Chem.* **1990**, *29*, 4429–4437.
[22] C. J. Siemer, F. A. Meece, W. H. Armstrong, D. M. Eichhorn, *Polyhedron* **2001**, *20*, 2637–2646.
[23] F. Hartmann, W. Kläui, A. Kremer-Aach, D. Mootz, A. Strerath, H. Wunderlich, *Z. Anorg. Allg. Chem.* **1993**, *619*, 2071–2076.
[24] J. S. Klitzke, T. Roisnel, J. F. Carpentier, O. L. Casagrande, *Inorg. Chim. Acta* **2009**, *362*, 4585–4592.

[25] N. Zhao, M. J. Van Stipdonk, C. Bauer, C. Campana, D. M. Eichhorn, *Inorg. Chem.* **2007**, *46*, 8662–8667.
[26] L. Müller, S. Hoof, M. Keck, C. Herwig, C. Limberg, *Chem. Eur. J.* **2020**, *26*, 11851–11861.
[27] F. A. Kunrath, R. F. De Souza, O. L. Casagrande, N. R. Brooks, V. G. Young, *Organometallics* **2003**, *22*, 4739–4743.
[28] M. Yoko, M. Kenji, *Catalyst for Olefin Oligomerizing, and Olefin Oligomerizing Method V*, **2009**, JP 2009172466.
[29] T. Kitano, Y. Sohrin, Y. Hata, H. Kawakami, T. Hori, K. Ueda, *J. Chem. Soc. Dalton Trans.* **2001**, 3564–3571.
[30] J. D. Oliver, B. B. Hutchinson, D. F. Mullica, W. O. Milligan, *Inorg. Chem.* **1980**, *19*, 165–169.
[31] M. R. Churchill, K. Gold, C. E. Maw, *Inorg. Chem.* **1970**, *9*, 1597–1604.
[32] G. Bandoni, D. A. Clemente, G. Paolucci, L. Doretti, *Cryst. Struct. Commun.* **1979**, *8*, 965.
[33] C. Santini, C. Pettinari, M. Pellei, G. Gioia Lobbia, A. Pifferi, M. Camalli, A. Mele, *Polyhedron* **1999**, *18*, 2255–2263.
[34] K. Nakata, S. Kawabata, K. Ichikawa, *Acta Crystallogr. Sect. C* **1995**, *51*, 1092–1094.
[35] S. Calogero, G. G. Lobbia, P. Cecchi, G. Valle, J. Friedl, *Polyhedron* **1994**, *13*, 87–97.
[36] W. K. Myers, E. N. Duesler, D. L. Tierney, *Inorg. Chem.* **2008**, *47*, 6701–6710.
[37] P. Cecchi, G. G. Lobbia, F. Marchetti, G. Valle, S. Calogero, *Polyhedron* **1994**, *13*, 2173–2178.
[38] H. X. Yong, K. Aoki, Y. B. Feng, *Synth. React. Inorg. Met.-Org. Chem.* **2004**, *34*, 1149–1163.
[39] M. D. Santana, L. López-Banet, G. García, L. García, J. Pérez, M. Liu, *Eur. J. Inorg. Chem.* **2008**, *2*, 4012–4018.
[40] N. Kitajima, Y. Moro-oka, A. Uchida, Y. Sasada, Y. Ohashi, *Acta Crystallogr. Sect. C* **1988**, *44*, 1876–1878.
[41] K.-W. Yang, Y.-Z. Wang, Z.-X. Huang, J. Sun, *Polyhedron* **1997**, *16*, 1297–1300.
[42] D. M. Eichhorn, W. H. Armstrong, *Inorg. Chem.* **1990**, *29*, 3607–3612.
[43] L. M. L. Chia, S. Radojevic, I. J. Scowen, M. McPartlin, M. A. Halcrow, *J. Chem. Soc. Dalton Trans.* **2000**, 133–140.
[44] S. Liang, H. Wang, T. Deb, J. L. Petersen, G. T. Yee, M. P. Jensen, *Inorg. Chem.* **2012**, *51*, 12707–12719.
[45] T. Ruman, Z. Ciunik, E. Szklanny, S. Wołowiec, *Polyhedron* **2002**, *21*, 2743–2753.
[46] T. Deb, G. T. Rohde, V. G. Young, M. P. Jensen, *Inorg. Chem.* **2012**, *51*, 7257–7270.
[47] A. L. Rheingold, C. B. White, S. Trofimenko, *Inorg. Chem.* **1993**, *32*, 3471–3477.
[48] L. Yang, D. R. Powell, R. P. Houser, *J. Chem. Soc. Dalton Trans.* **2007**, 955–964.
[49] A. W. Addison, T. N. Rao, *Dalton Trans.* **1984**, 1349–1356.
[50] R. D. Shannon, *Acta Crystallogr. Sect. A* **1976**, *32*, 751–767.
[51] D. Reinen, C. Friebel, *Inorg. Chem.* **1984**, *23*, 791–798.
[52] R. G. Pearson, *J. Mol. Struct.: THEOCHEM* **1983**, *103*, 24–34.
[53] I. B. Bersuker, *Chem. Rev.* **2001**, *101*, 1067–1114.
[54] D. Reinen, M. Atanasov, *Chem. Phys.* **1989**, *136*, 27–46.
[55] D. Reinen, M. Atanasov, *Chem. Phys.* **1991**, *155*, 157–171.
[56] D. W. Meek, J. A. Ibers, *Inorg. Chem.* **1970**, *9*, 465–470.
[57] I. A. Guzei, M. Wendt, *J. Chem. Soc. Dalton Trans.* **2006**, 3991–3999.
[58] I. R. Crossley, *Adv. Organomet. Chem.* **2008**, *56*, 199–321.
[59] M. Brookhart, M. L. H. Green, G. Parkin, *Proc. Natl. Acad. Sci. USA* **2007**, *104*, 6908–6914.
[60] W. Scherer, A. C. Dunbar, J. E. Barquera-Lozada, D. Schmitz, G. Eickerling, D. Kratzert, D. Stalke, A. Lanza, P. Macchi, N. P. M. Casati, J. Ebad-Allah, C. Kuntsch, *Angew. Chem. Int. Ed.* **2015**, *54*, 2505–2509; *Angew. Chem.* **2015**, *127*, 2535–2539.
[61] W.-S. Ojo, K. Jacob, E. Despagnet-Ayoub, B. K. Muñoz, S. Gonell, L. Vendier, V. H. Nguyen, M. Etienne, *Inorg. Chem.* **2012**, *51*, 2893–2901.
[62] T. J. Swift, R. E. Connick, *J. Chem. Phys.* **1962**, *37*, 307–320.
[63] J. D. Satterlee, *Concepts Magn. Reson.* **1990**, *2*, 119–129.
[64] A. J. Pell, G. Pintacuda, C. P. Grey, *Prog. Nucl. Magn. Reson. Spectrosc.* **2019**, *111*, 1–271.
[65] A. Pyykkönen, R. Feher, F. H. Köhler, J. Vaara, *Inorg. Chem.* **2020**, DOI 10.1021/acs.inorgchem.0c01176.
[66] P. J. Desrochers, J. Telser, S. A. Zvyagin, A. Ozarowski, J. Krzystek, D. A. Vicic, *Inorg. Chem.* **2006**, *45*, 8930–8941.
[67] T. Chávez-Gil, D. L. Cedeño, C. G. Hamaker, M. Vega, J. Rodriguez, *J. Mol. Struct.* **2008**, *888*, 168–172.
[68] S. Hoof, C. Limberg, *Z. Anorg. Allg. Chem.* **2019**, *645*, 170–174.
[69] W. S. Sheldrick, *SADABS*, University Of Göttingen, Germany, **1996**.
[70] W. S. Sheldrick, *Acta Crystallogr. Sect. A* **2015**, *71*, 3–8.
[71] W. S. Sheldrick, *Acta Crystallogr. Sect. C* **2015**, *71*, 3–8.
[72] A. L. Spek, *Acta Crystallogr. Sect. D* **2009**, *65*, 148–155.

Manuscript received: September 23, 2020
Revised manuscript received: October 30, 2020
Accepted manuscript online: November 3, 2020